

Figure 1A A simplified PSK transmitter.

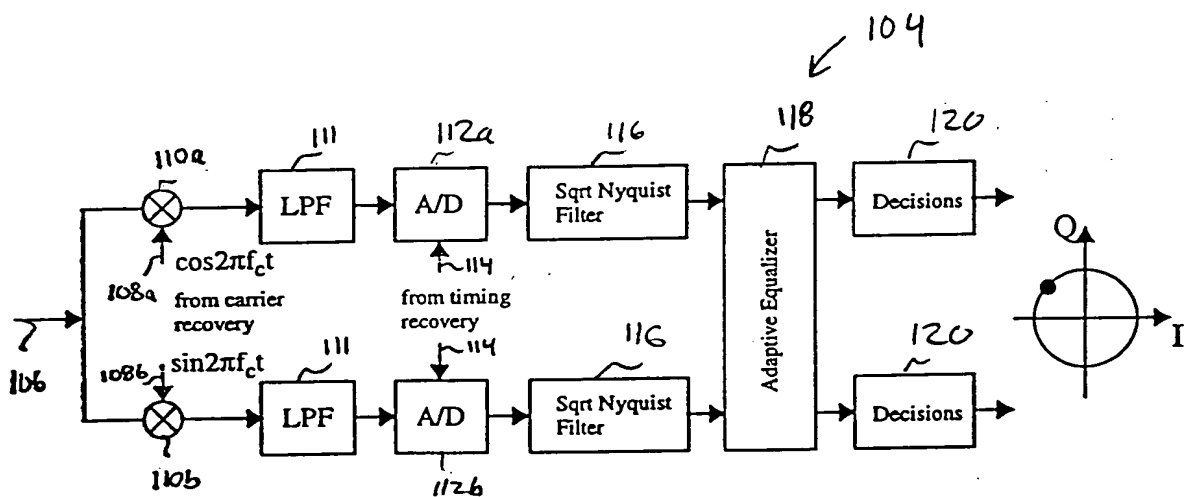


Figure 1B A simplified PSK receiver.

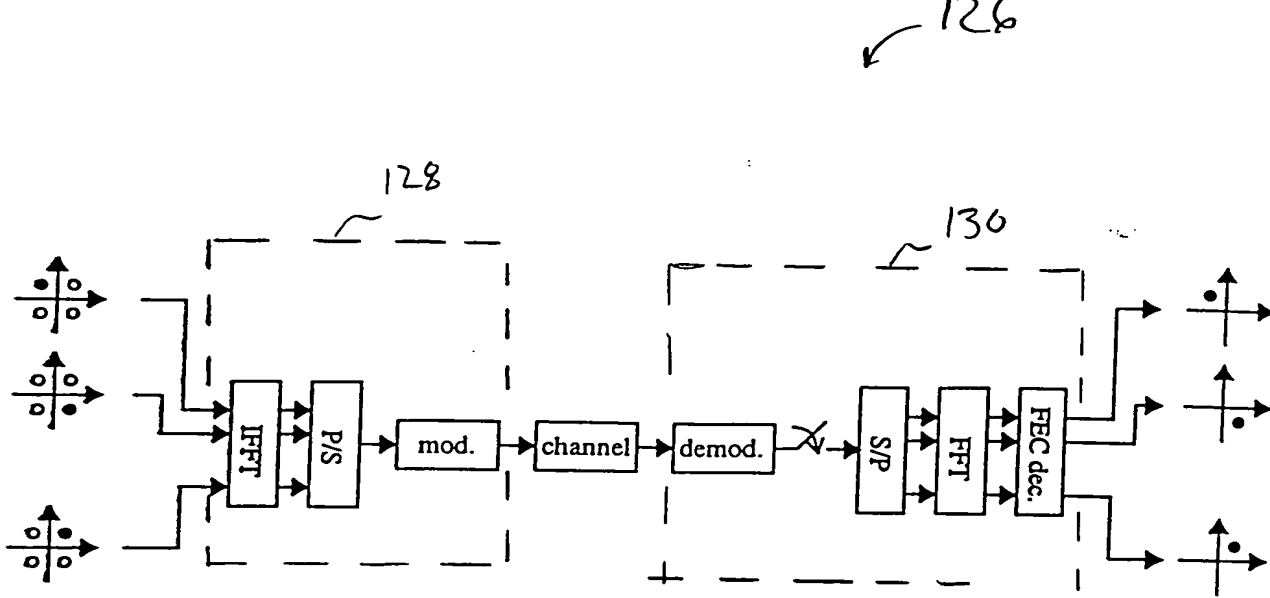


Figure 1C Simplified block diagram of an OFDM system.

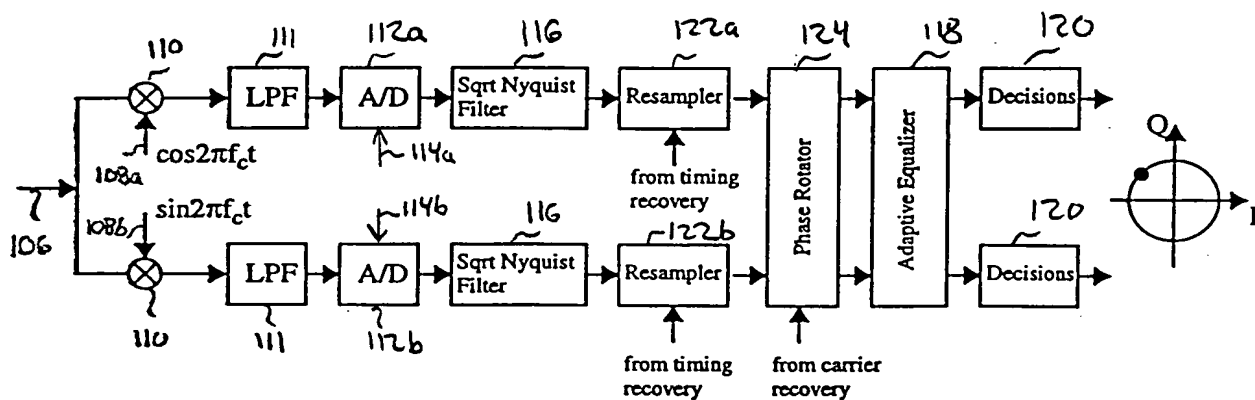


Figure 1D PSK receiver with carrier and timing recovery.

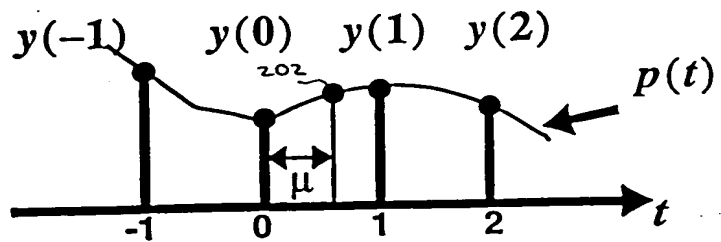
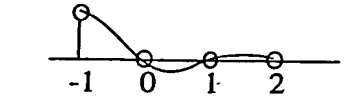
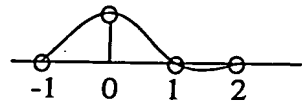


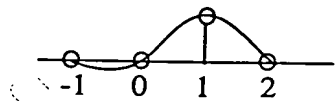
Figure 2 Interpolation Environment



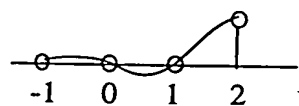
$$C_{-1}(\mu) = -\frac{1}{6}\mu^3 + \frac{1}{2}\mu^2 - \frac{1}{3}\mu$$



$$C_0(\mu) = \frac{1}{2}\mu^3 - \mu^2 - \frac{1}{2}\mu + 1$$



$$C_1(\mu) = \frac{1}{2}\mu^3 + \frac{1}{2}\mu^2 + \mu$$



$$C_2(\mu) = \frac{1}{6}\mu^3 - \frac{1}{6}\mu$$

Figure 3 The Lagrange basis polynomials.

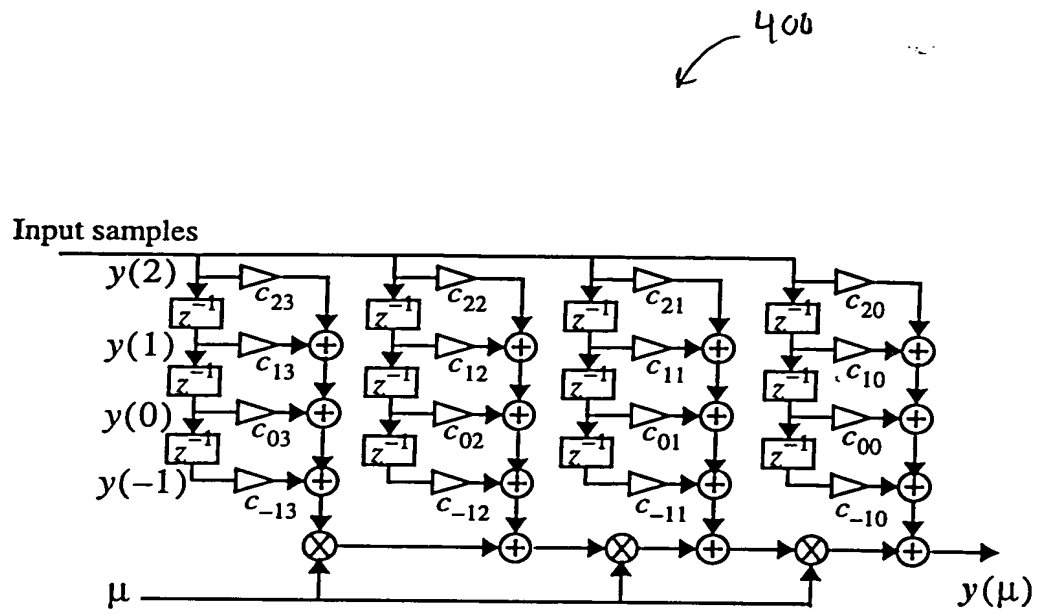


Figure 4 The Farrow structure that implements (2.5) and (2.6).

00000000=64285760

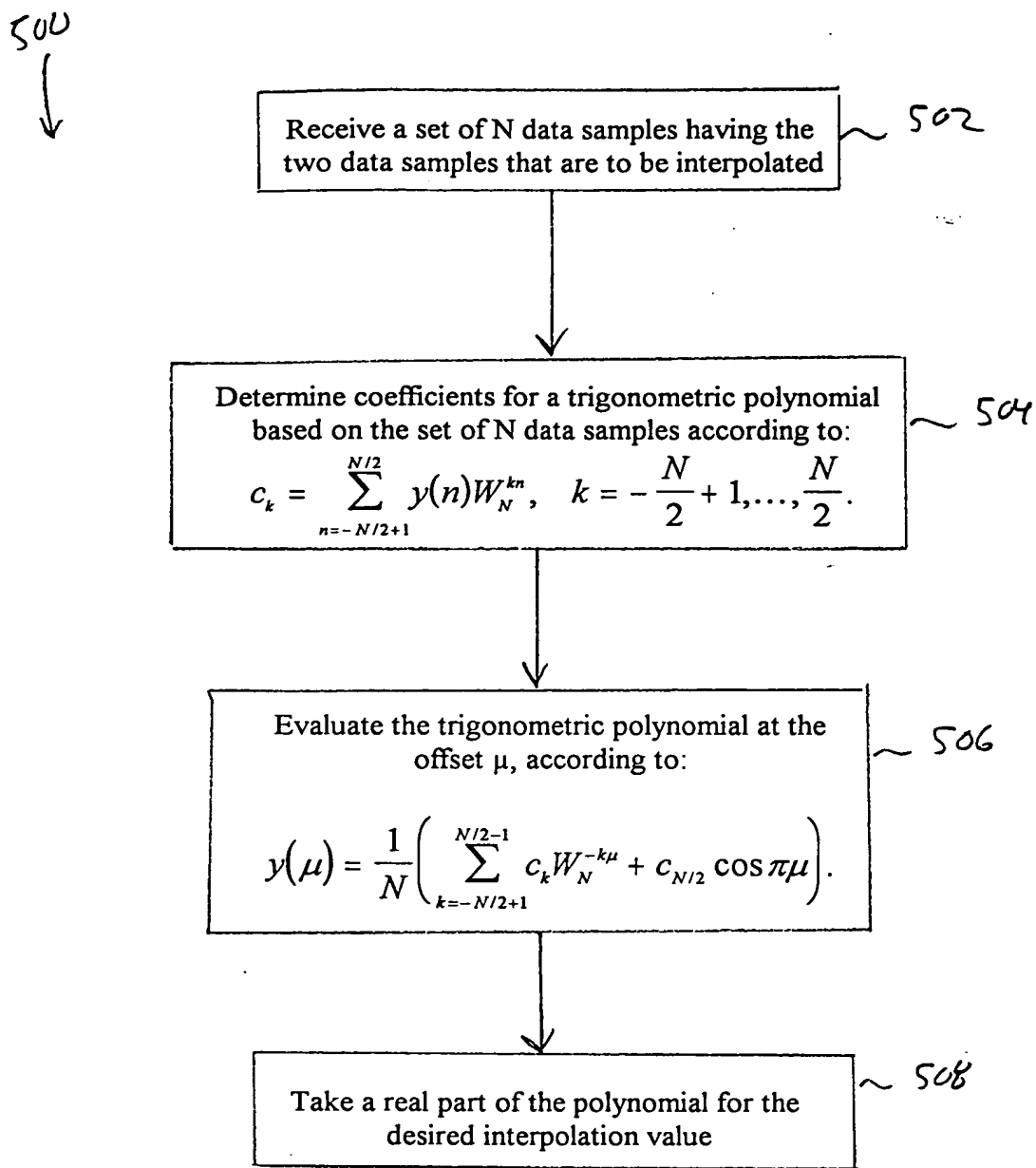


FIG. 5

FIG. 6A

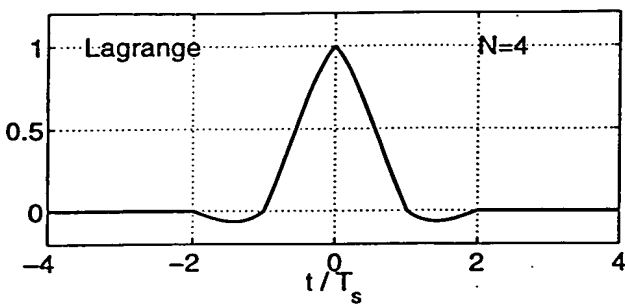


FIG. 6B

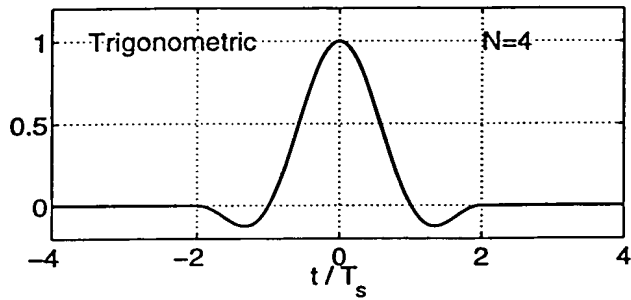


FIG. 6A - 6B Impulse responses of (a) Lagrange interpolator and (b) Trigonometric interpolator.

FIG. 7A

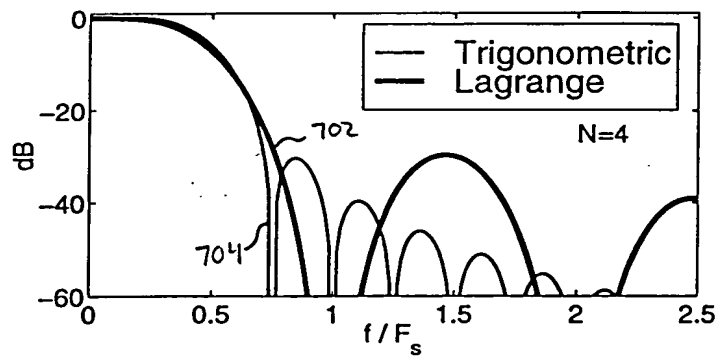


FIG. 7B

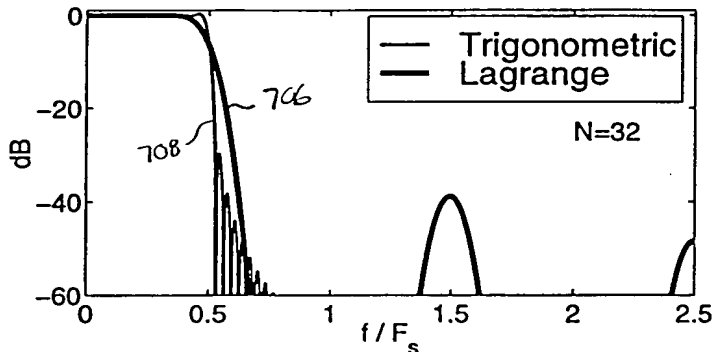


FIG. 7A-7B: Frequency responses for (a)  $N=4$  and (b)  $N=32$ .

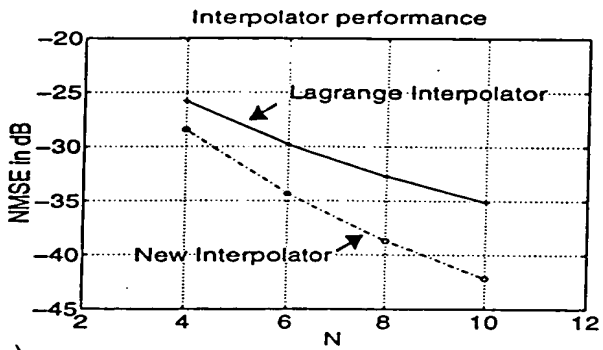


Figure 8B NMSE of the interpolated signal.

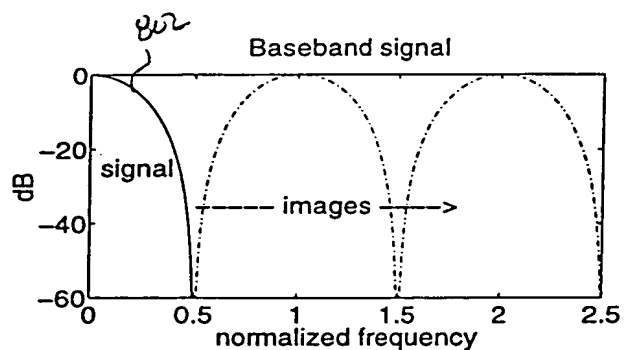


Figure 8A Signal with two samples/symbol and 100% excess BW.

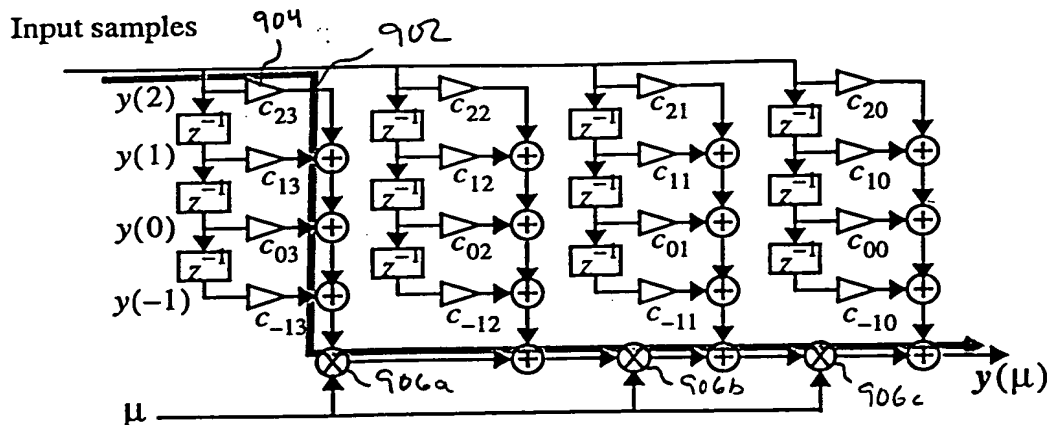


Figure 9 The critical path of the Lagrange cubic interpolator.

$\curvearrowleft$   $loc$

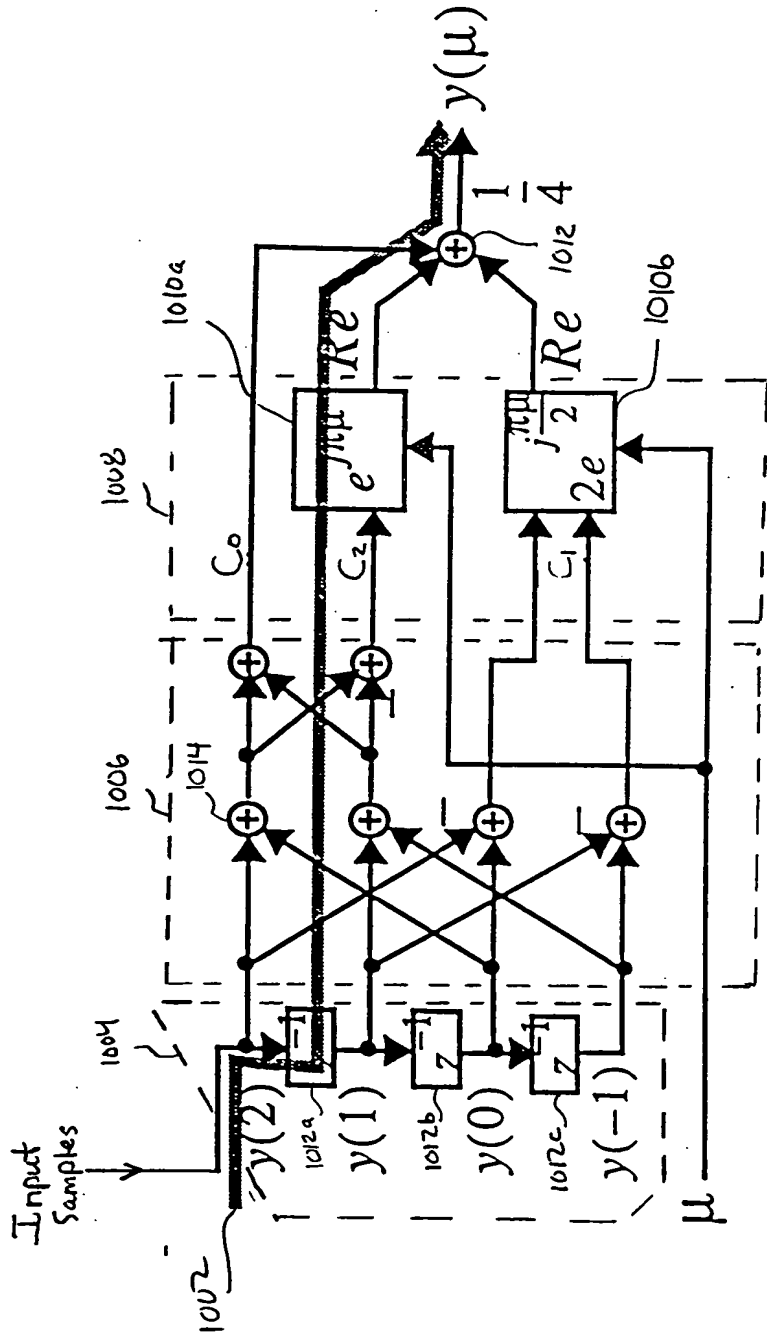


FIG. 10: Trigonometric Interpolator ( $N=4$ )

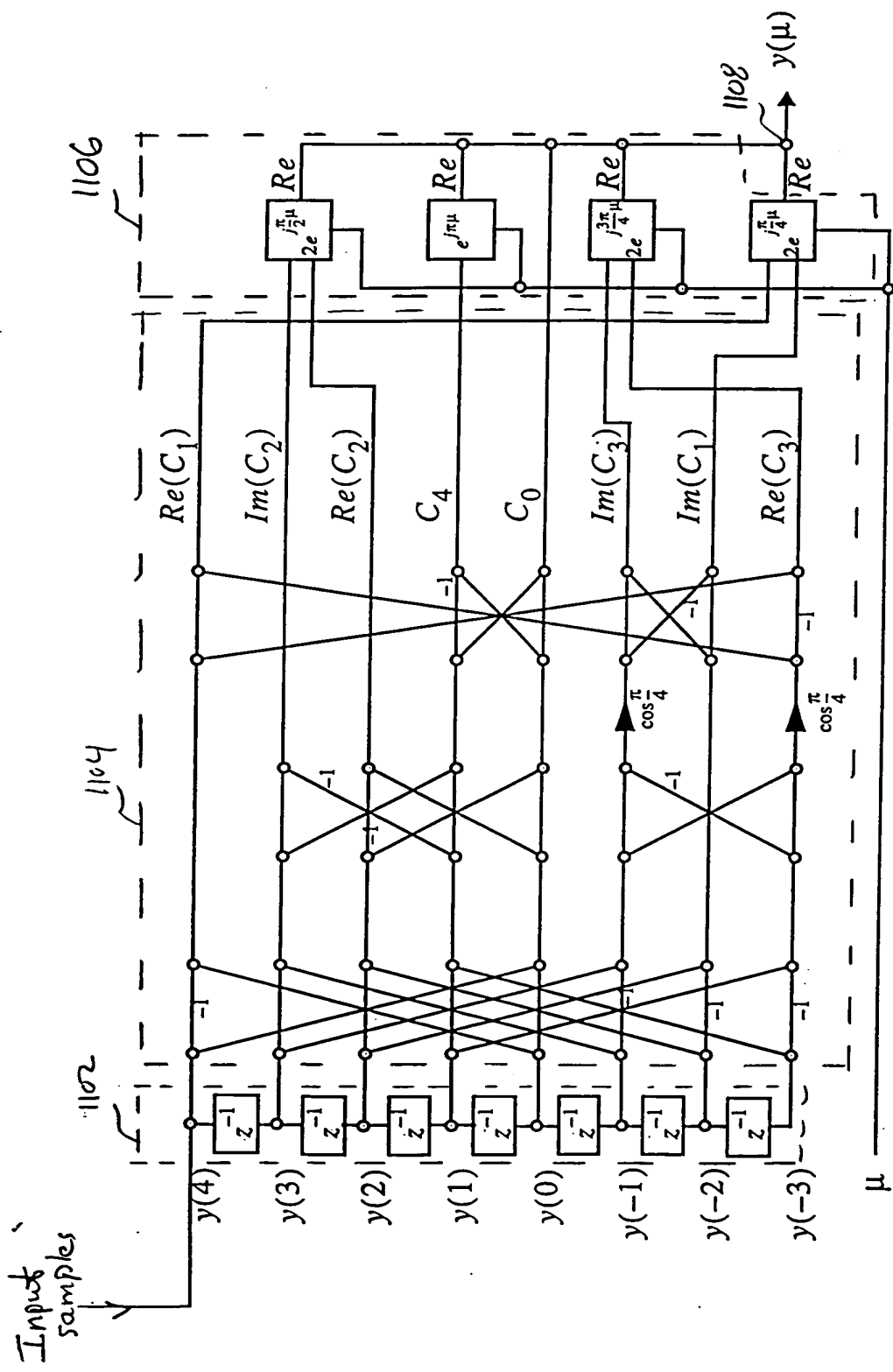


Figure 11 Trisomic Interpolator with  $N=8$ .

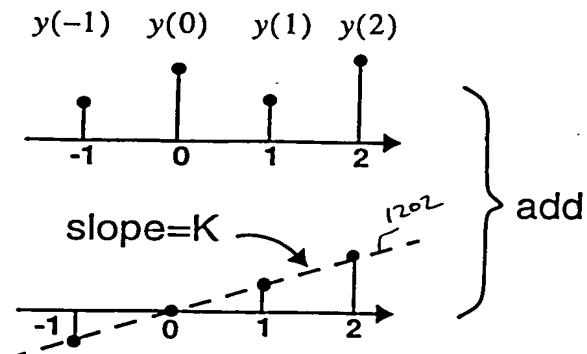


Figure 12 Conceptual modification of input samples.

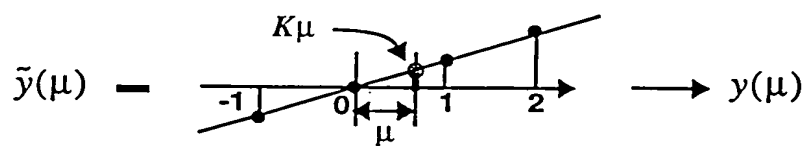


Figure 13 Correcting the offset due to modification of original samples.

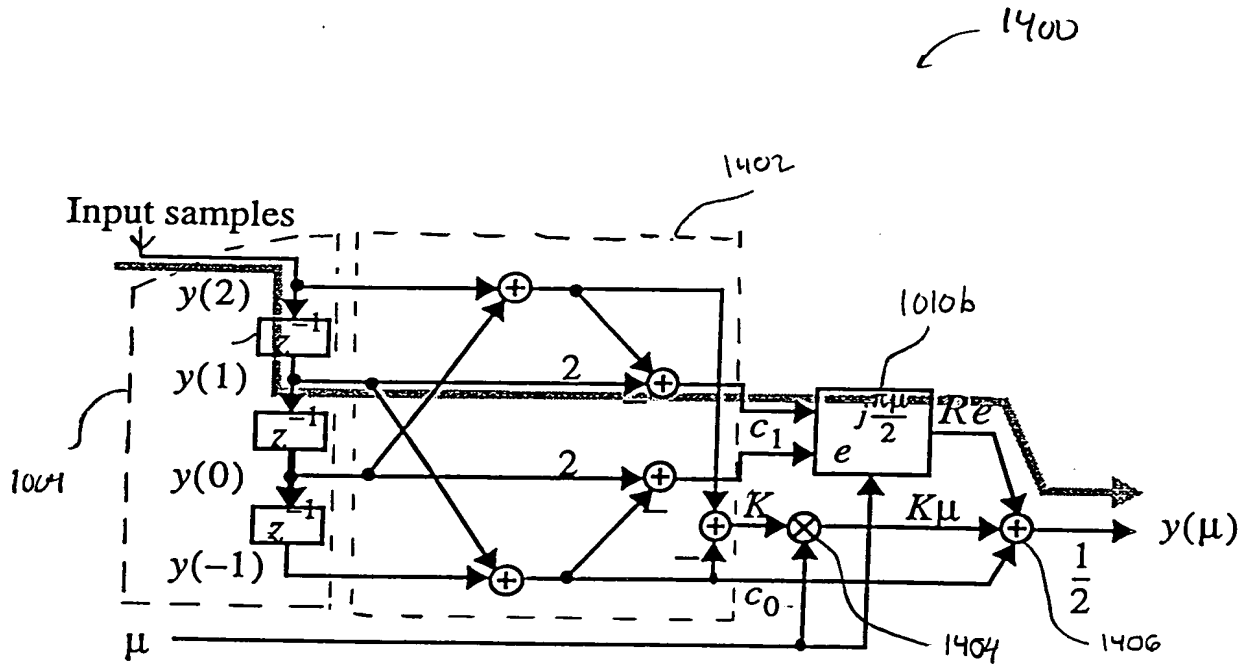


FIG. 14: Trigonometric Interpolator  $N=4$

1500

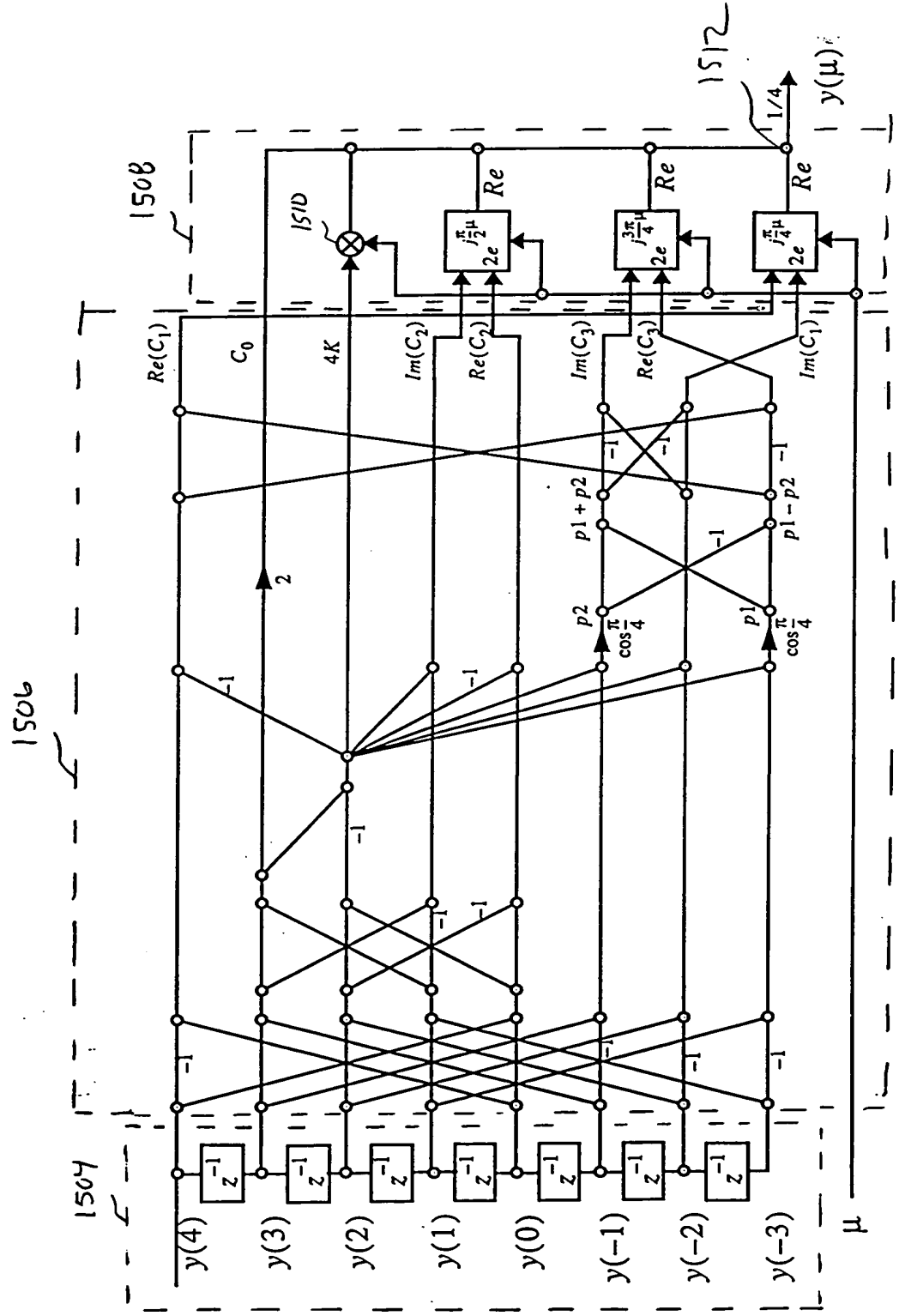


FIG. 15 The modified Trigonometric Interpolator

Interpolation errors are shown in gray.

FIG. 16A: Lagrange cubic

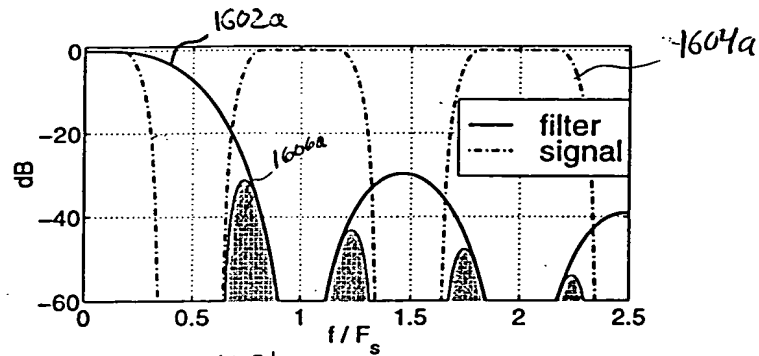


FIG. 16B: Trigonometric Interpolator 1000 (FIG. 10)

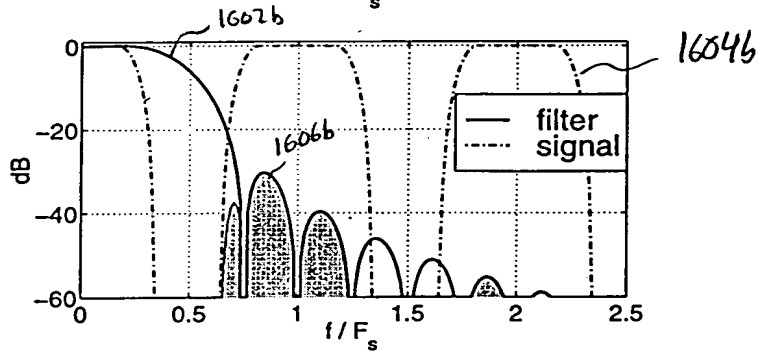


FIG. 16C: Trigonometric Interpolator 1400 (FIG. 14)

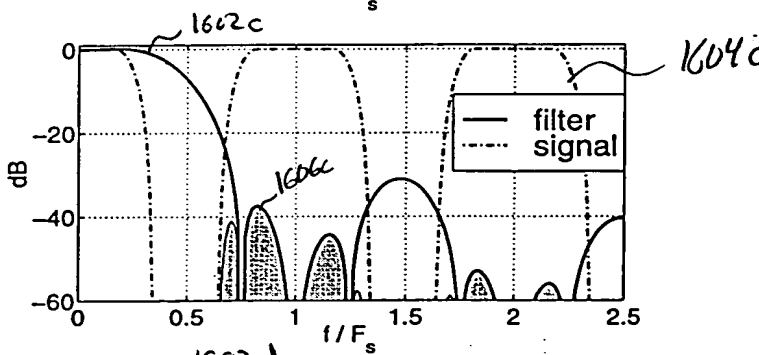
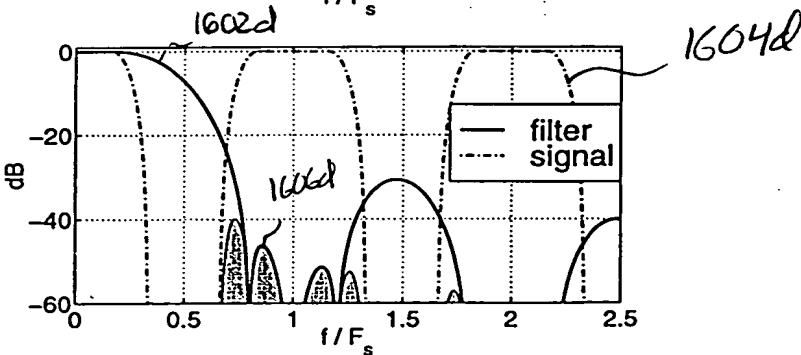


FIG. 16D: Optimal structure



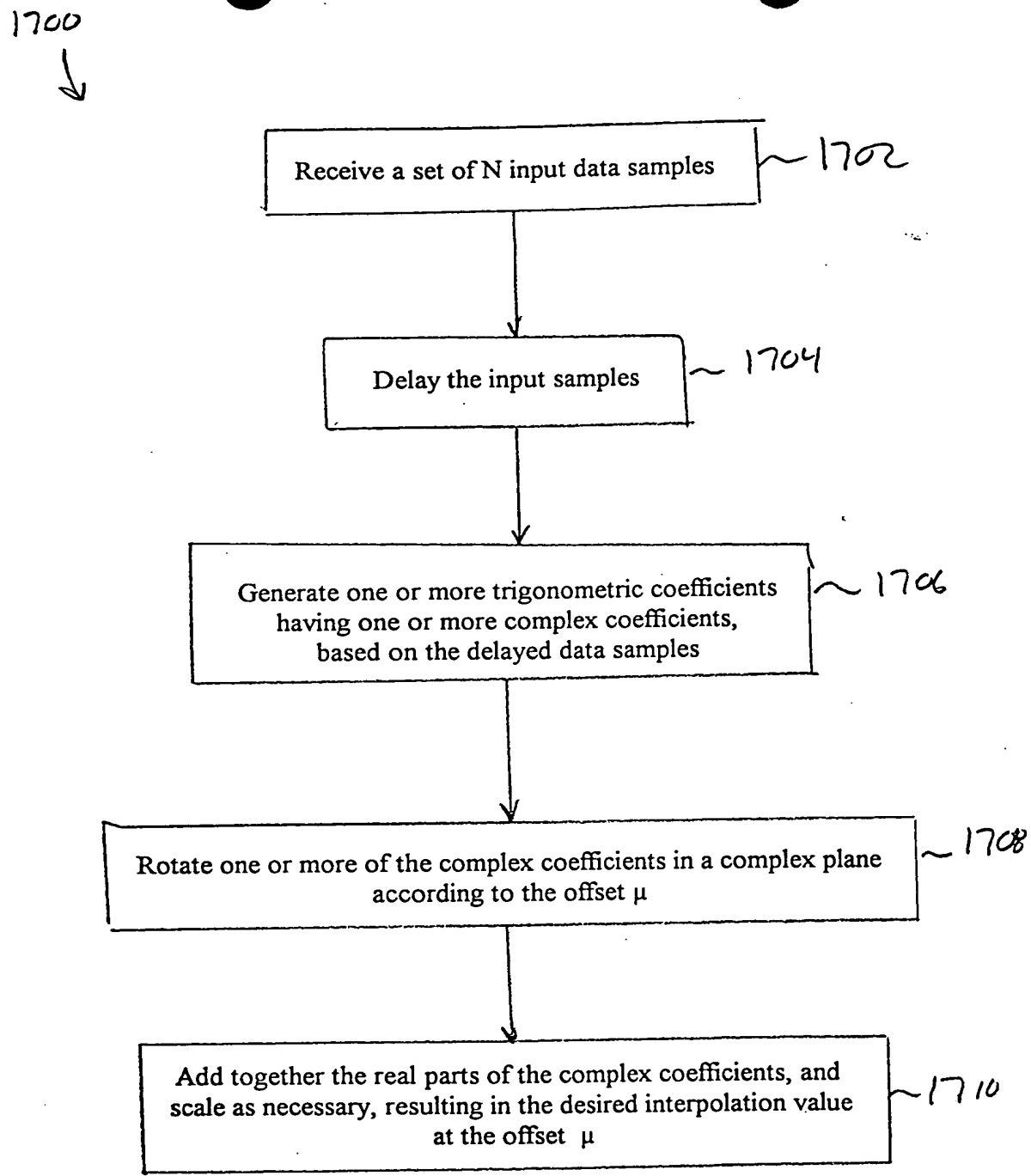


FIG. 17

0000111011001100

1800  
↙

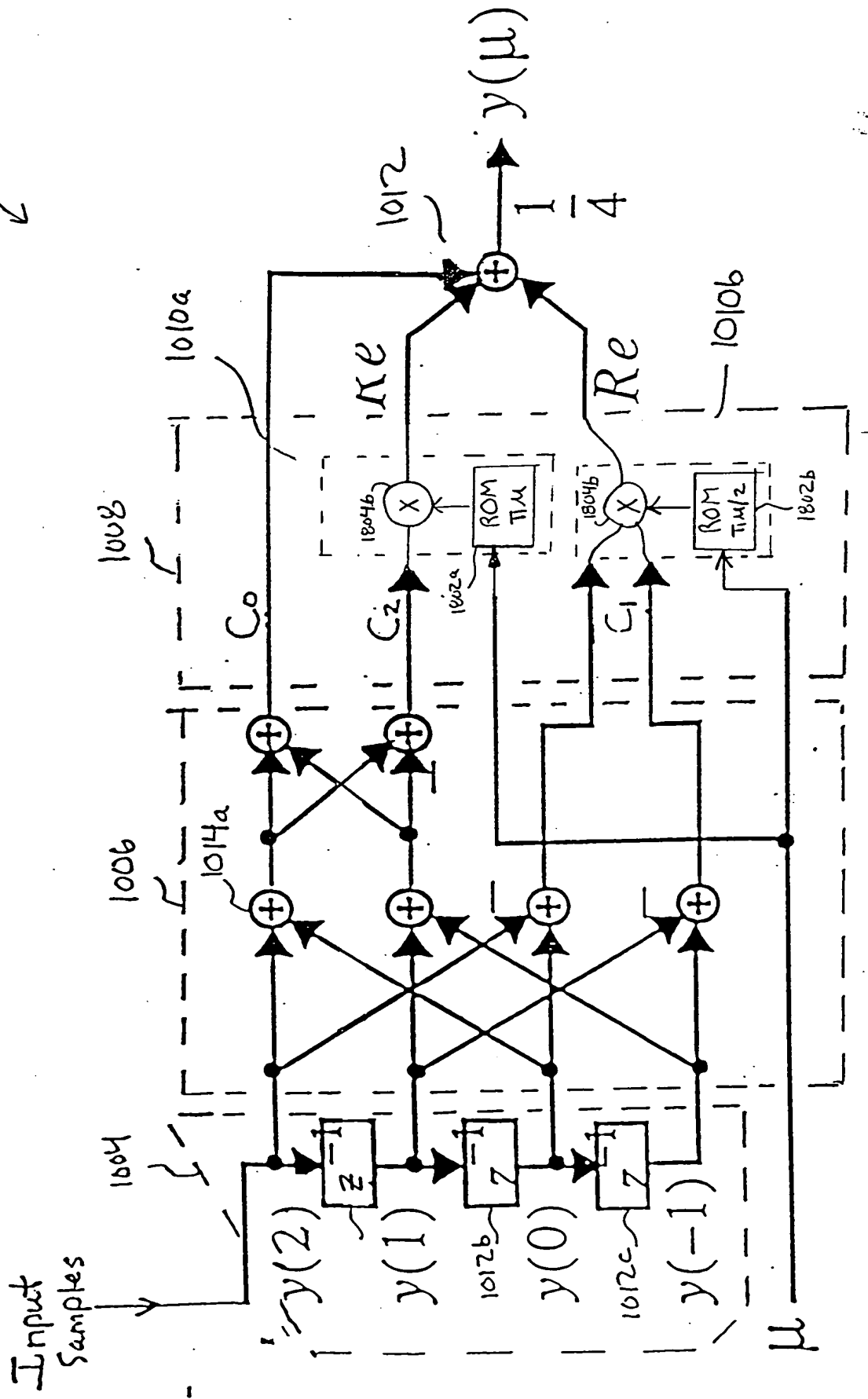


FIG. 18

DEC 24 1960

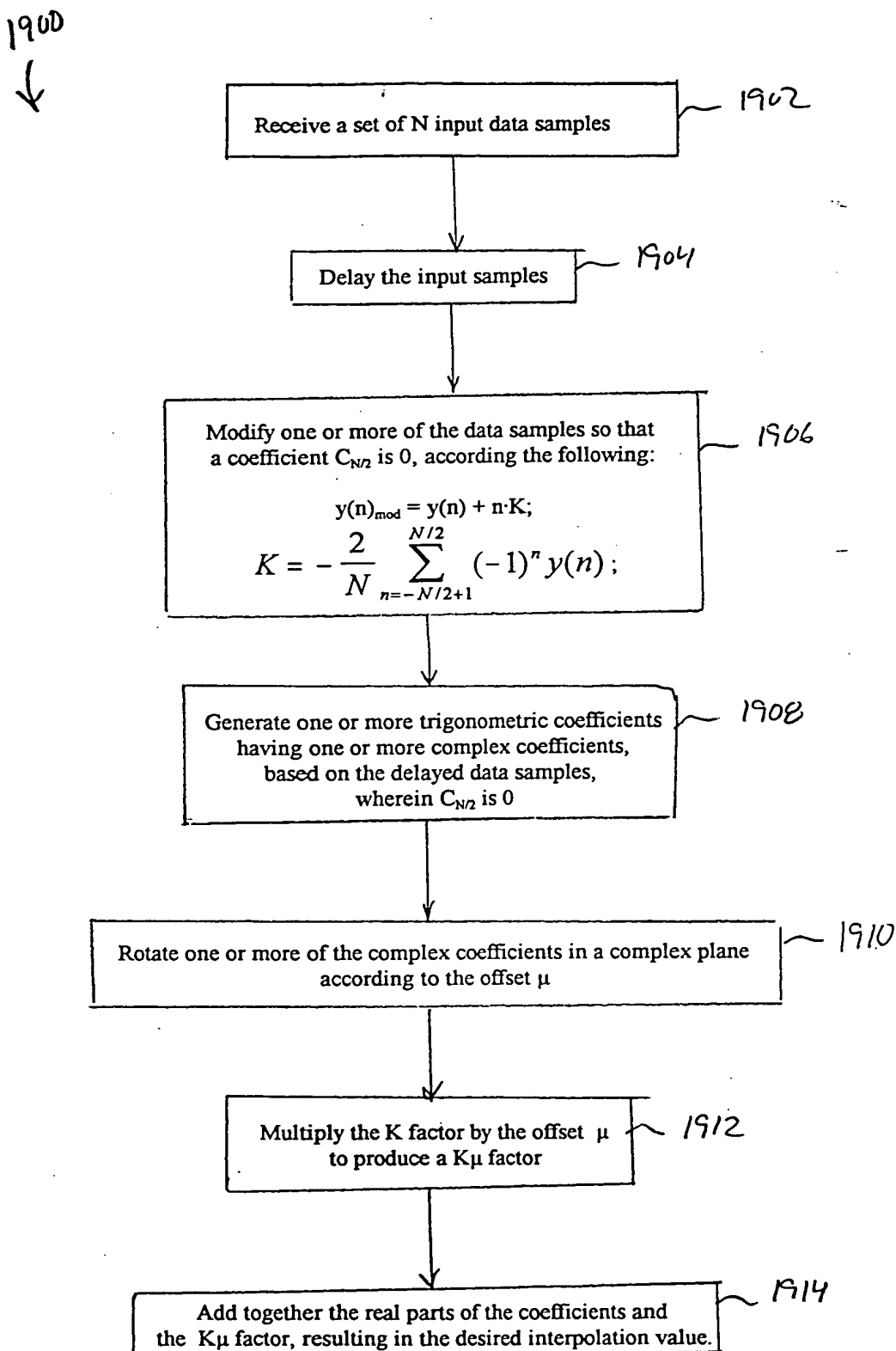


FIG. 19

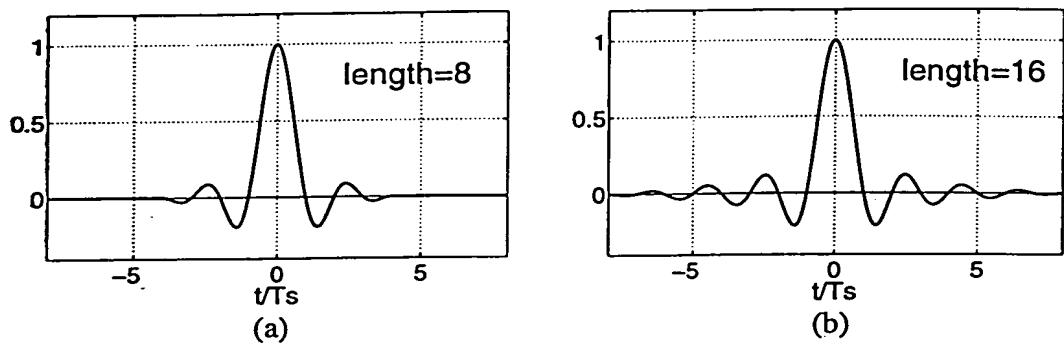


FIG. 20: Normalized Impulse responses  $f$  of the interpolation filters.

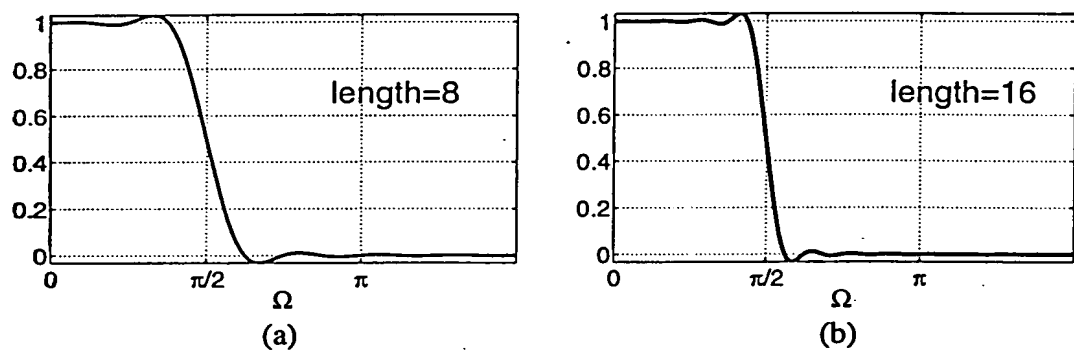


FIG. 21: Normalized Frequency responses  $F$  of the interpolation filters.

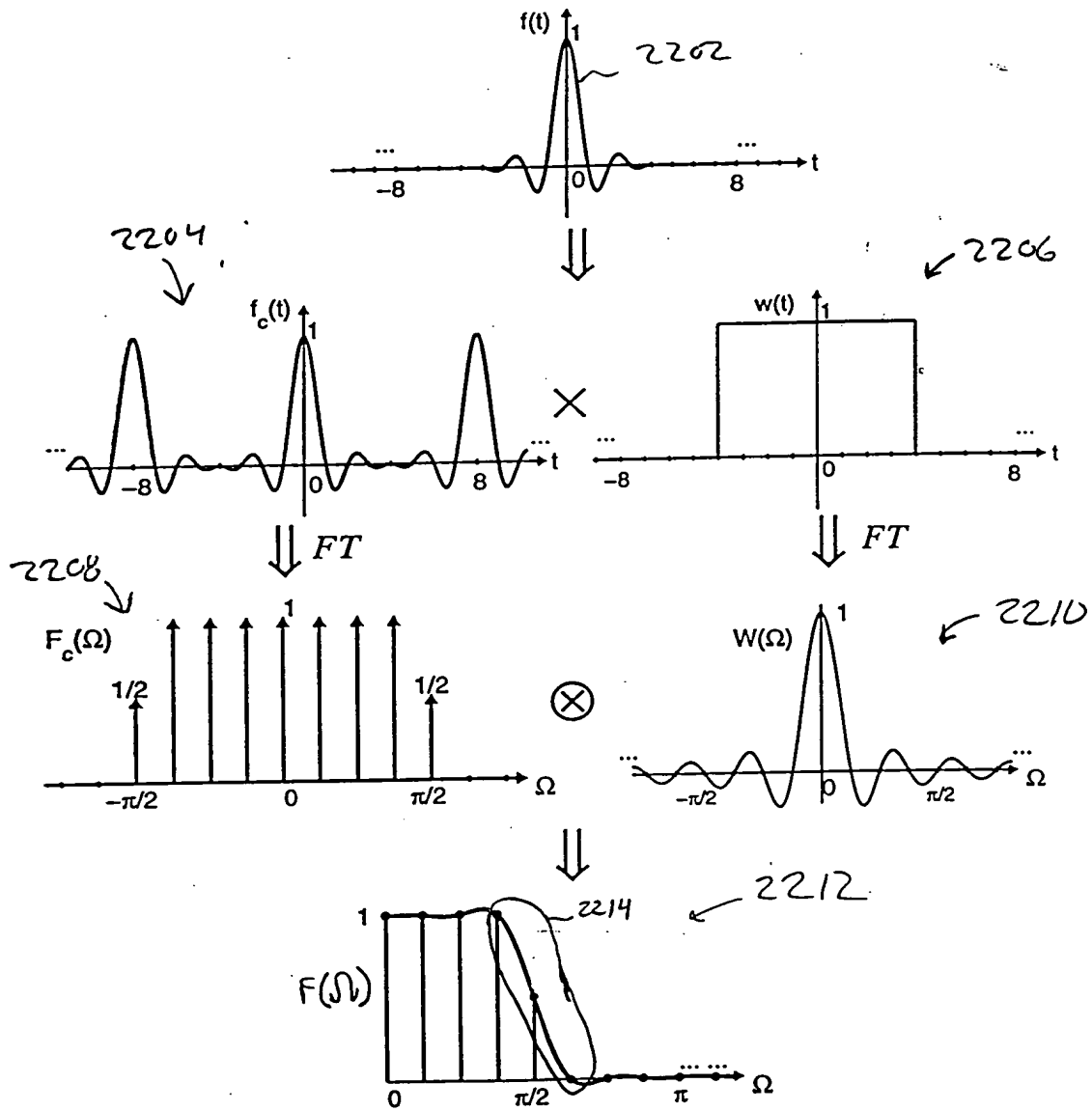


FIG.22: Analysis of the frequency responses.

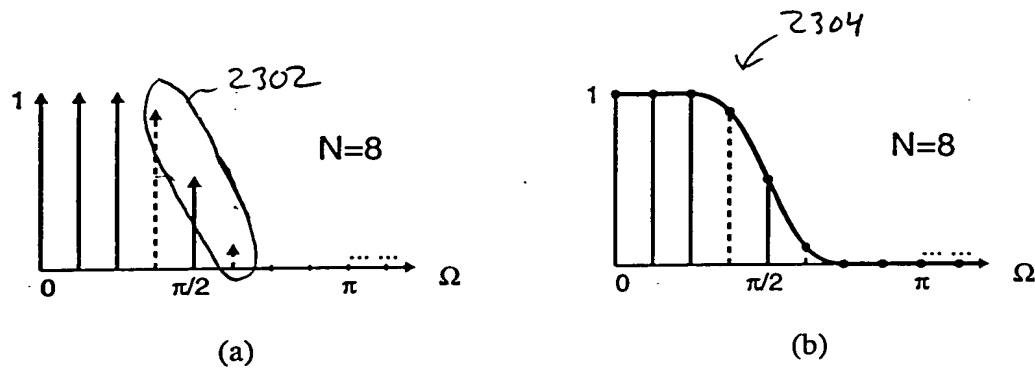
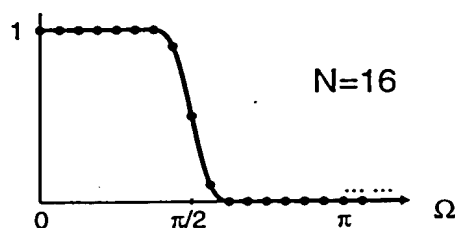


FIG. 23 Effect of a more gradual transition at the band edge.



**FIG. 24** Reducing the transition bandwidth by increasing  $N$ .

3-4b, in which  $N = 8$ .

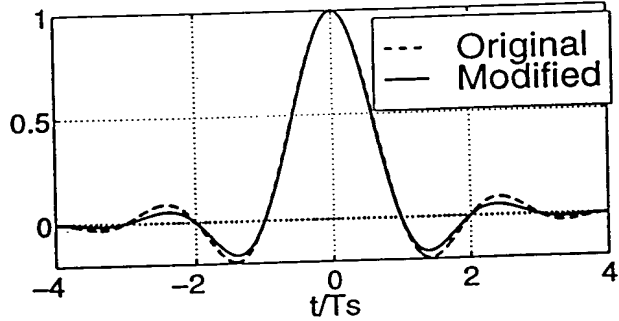


FIG.25A

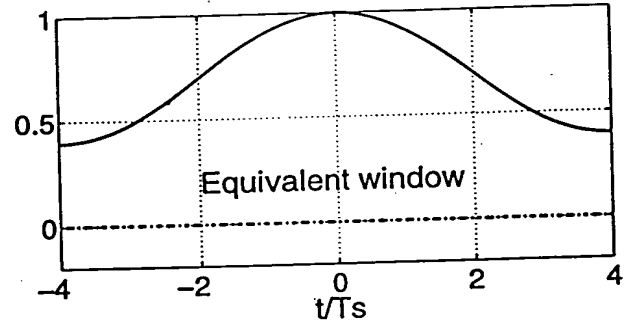


FIG.25B

FIG.25A-B: (A) Impulse response of the original filter and the modified filter; (B) The equivalent window.

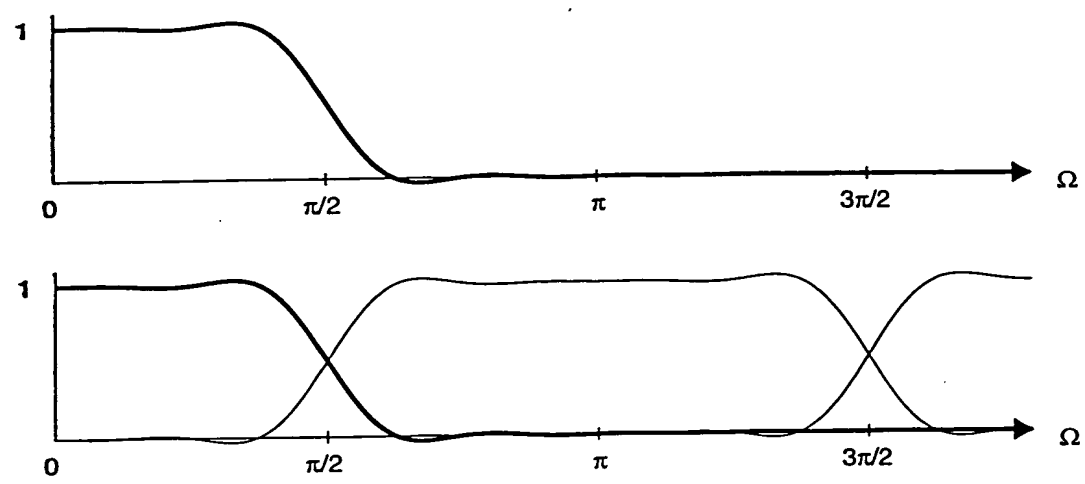


Fig. 26 Forming the frequency response of the discrete-time fractional-delay filter.

FIG. 27A

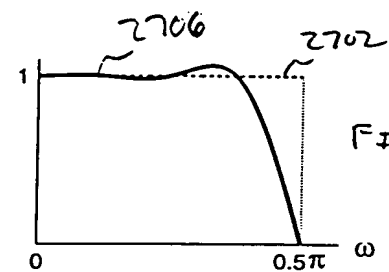
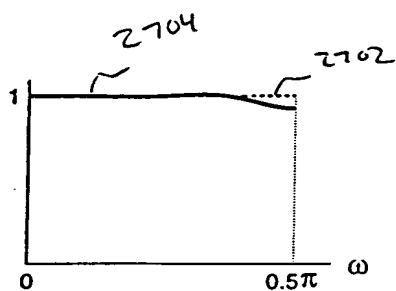
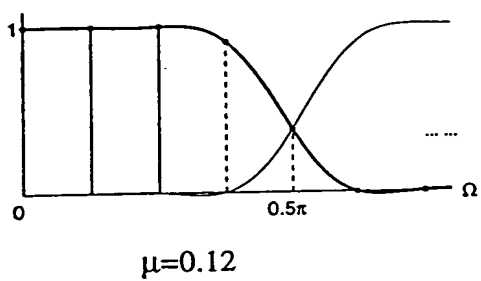


FIG. 27B

FIG. 27A-B : Fractional-delay filter with (A)  $\mu=0.12$  and (B)  $\mu=0.5$ , using the preliminary  $N=8$  interpolator.

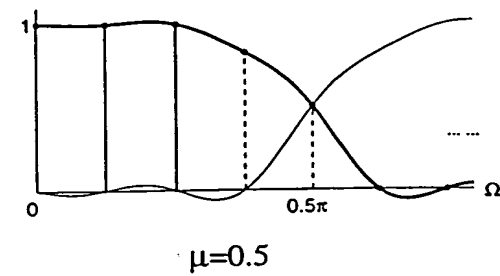
09692449 - 403000

FIG. 28A



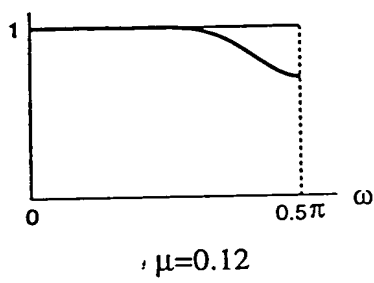
$\mu=0.12$

FIG. 28B



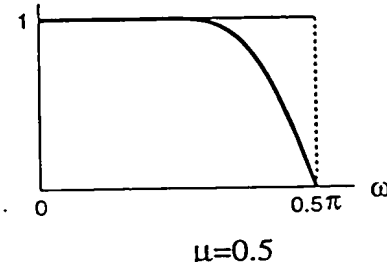
$\mu=0.5$

FIG. 28C



$\mu=0.12$

FIG. 28D



$\mu=0.5$

FIG. 29A

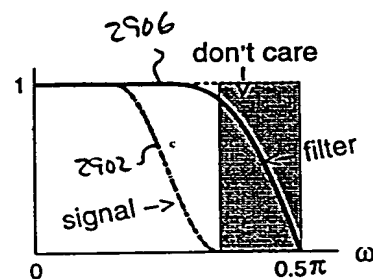
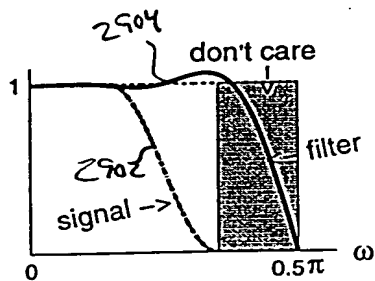


FIG. 29A-B :  $F_\mu(\omega)$ , with  $\mu=0.5$ ,  $N=8$ , (A) before and (B) after optimization.

Date: 04/26/2020

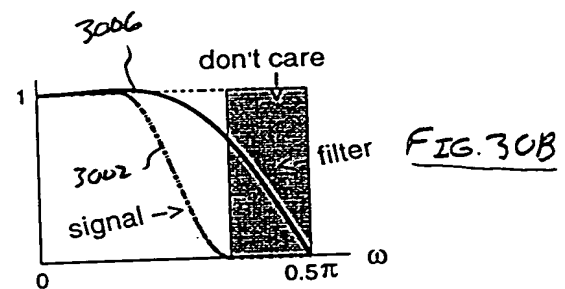
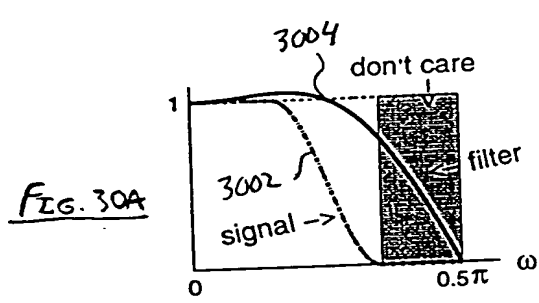


FIG. 30A-B  $F_\mu(\omega)$  for  $\mu=0.5$ ,  $N=4$ , A: before and B: after modification.

000207 64286960

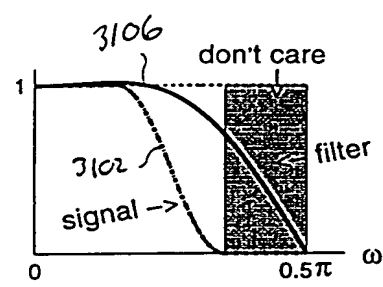
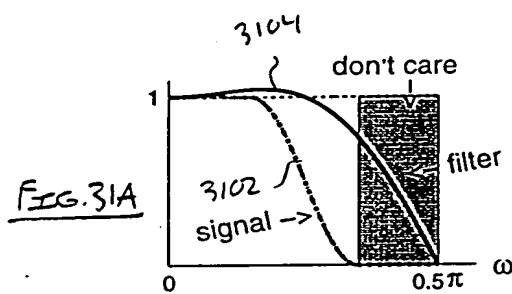


FIG. 31A-B  $F_\mu(\omega)$ ,  $\mu=0.5$ , simplified  $N=4$  structure, A' before and 'B, after modification.

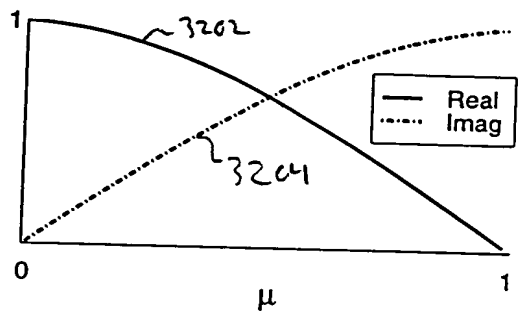


FIG.32: Real and imaginary components of the  $F_{\mu}(1)e^{j\frac{\pi}{2}\mu}$  value.

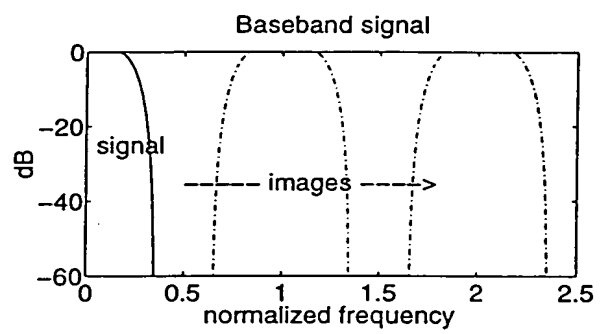


FIG.33: Signal with two samples/symbol and 40% excess bandwidth.

00000000000000000000000000000000

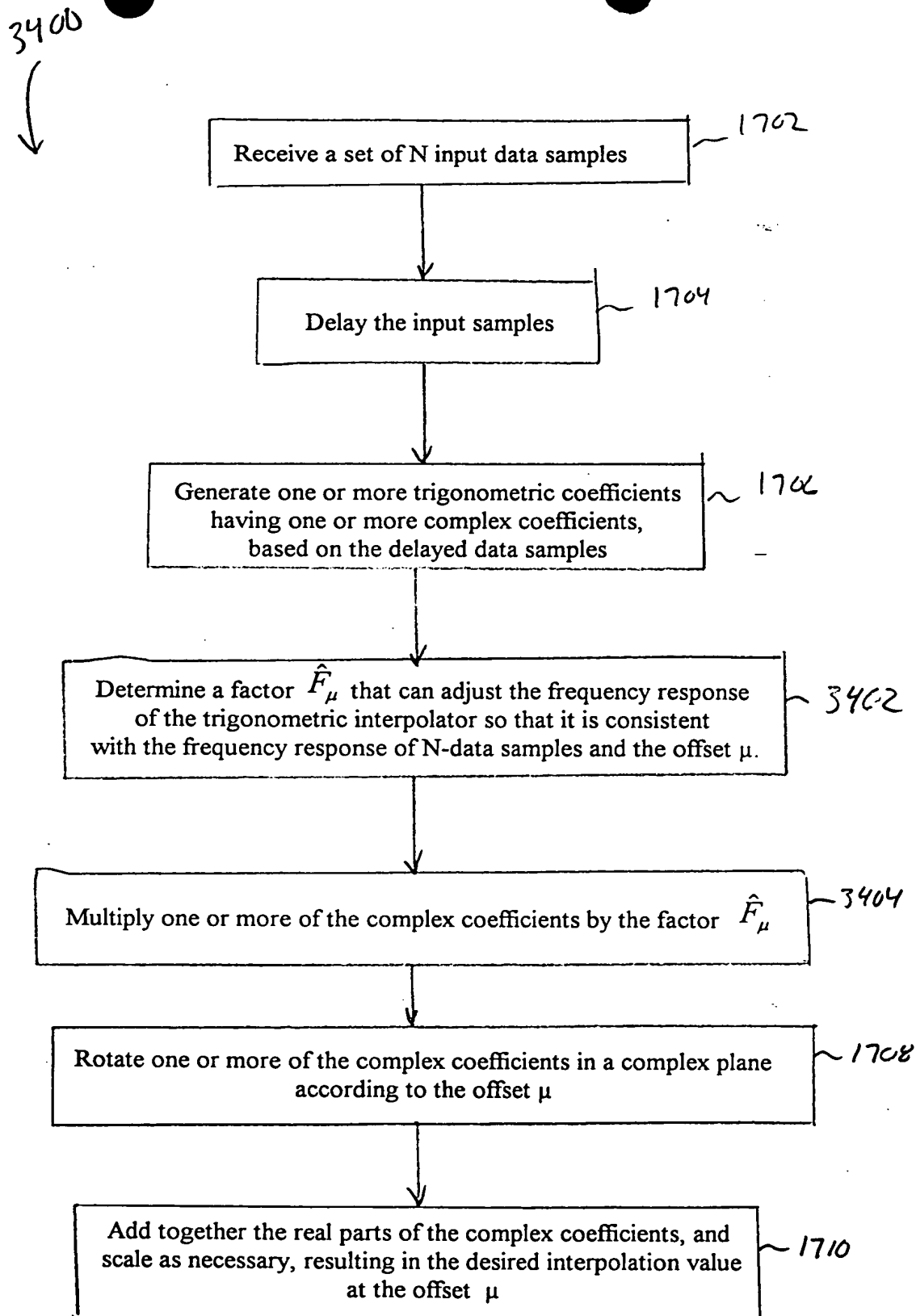


Fig. 341

0969364242442000

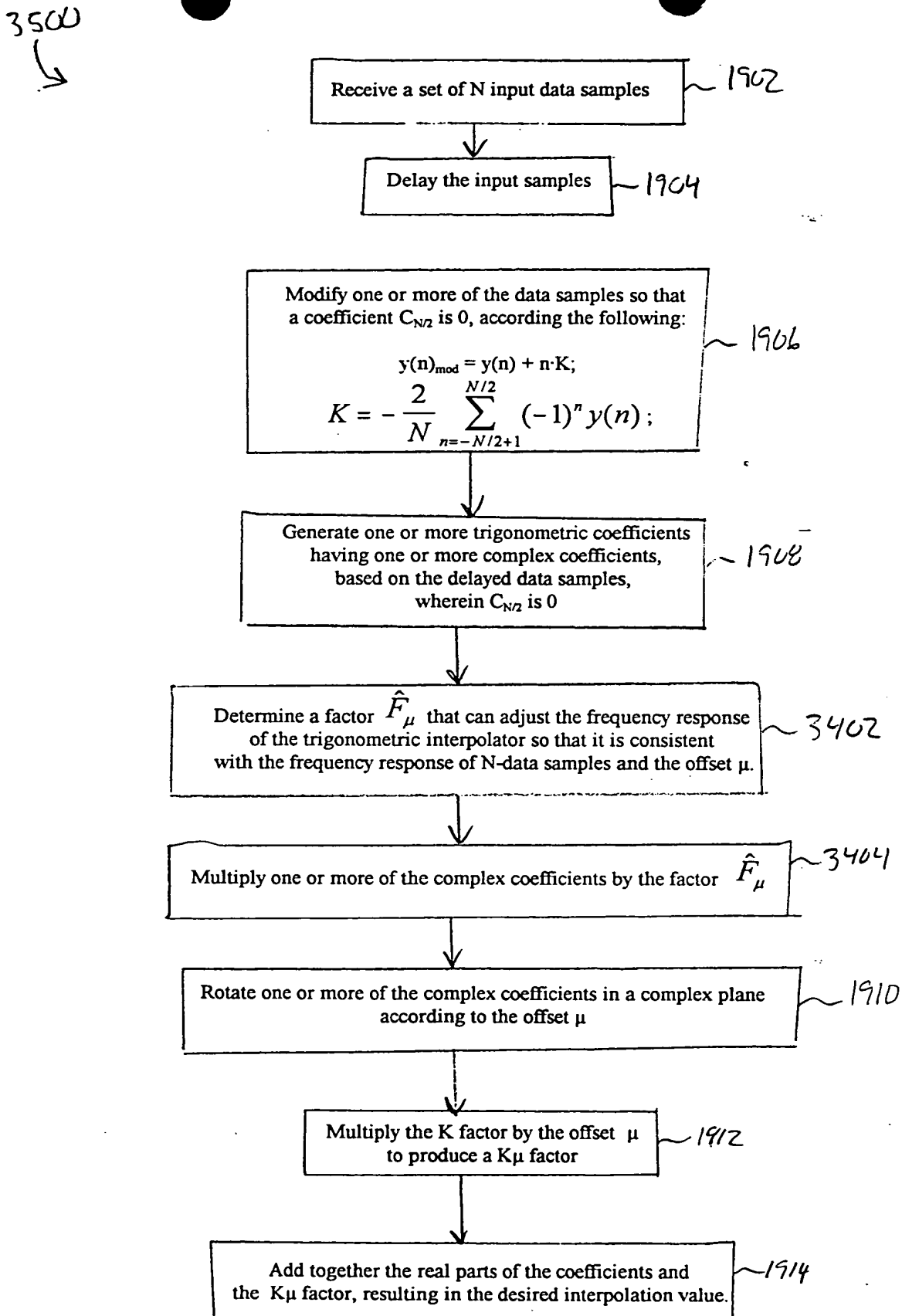


FIG. 35

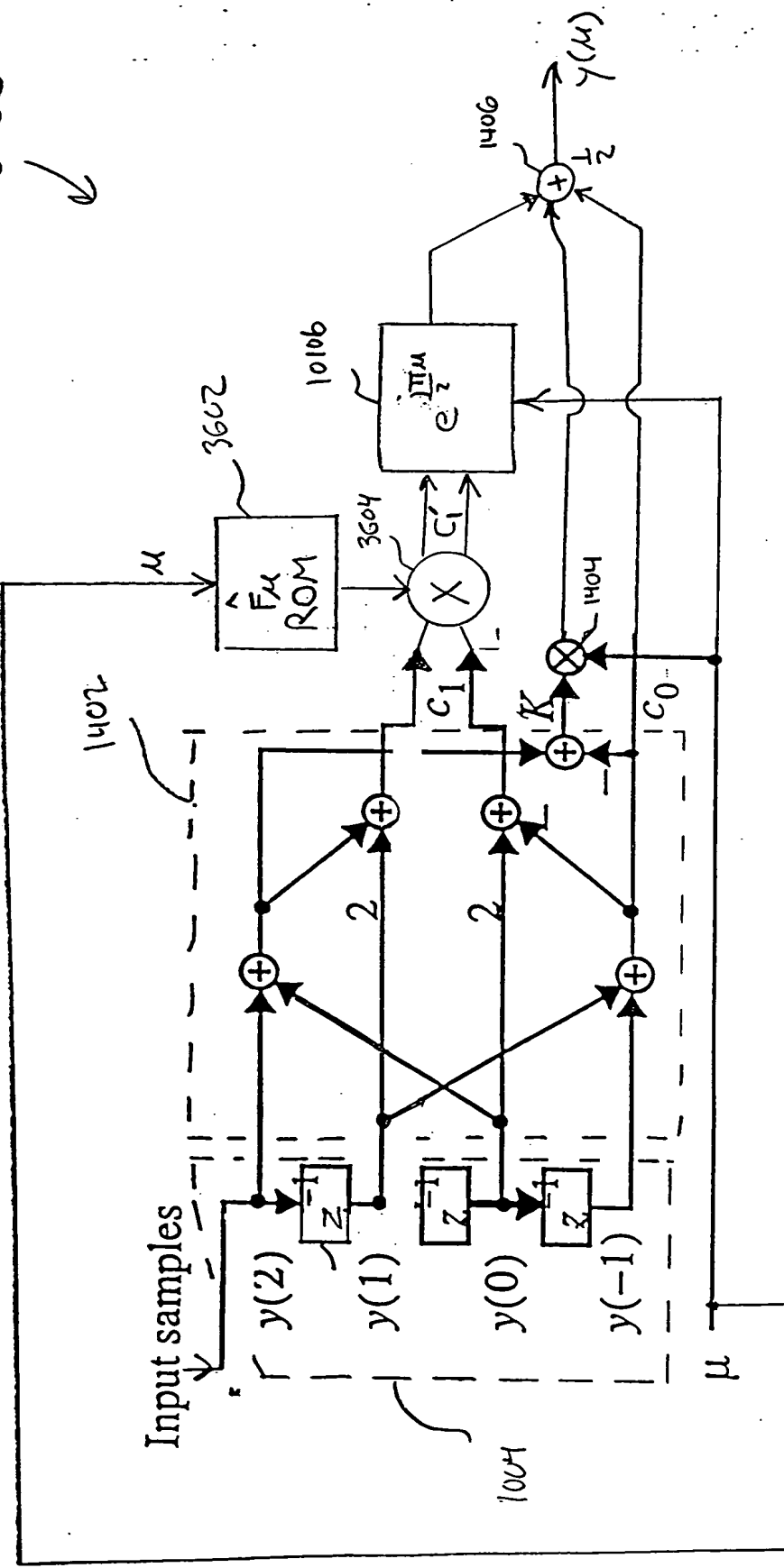


Fig. 36 The optimized structure for  $N=4$ .

3700

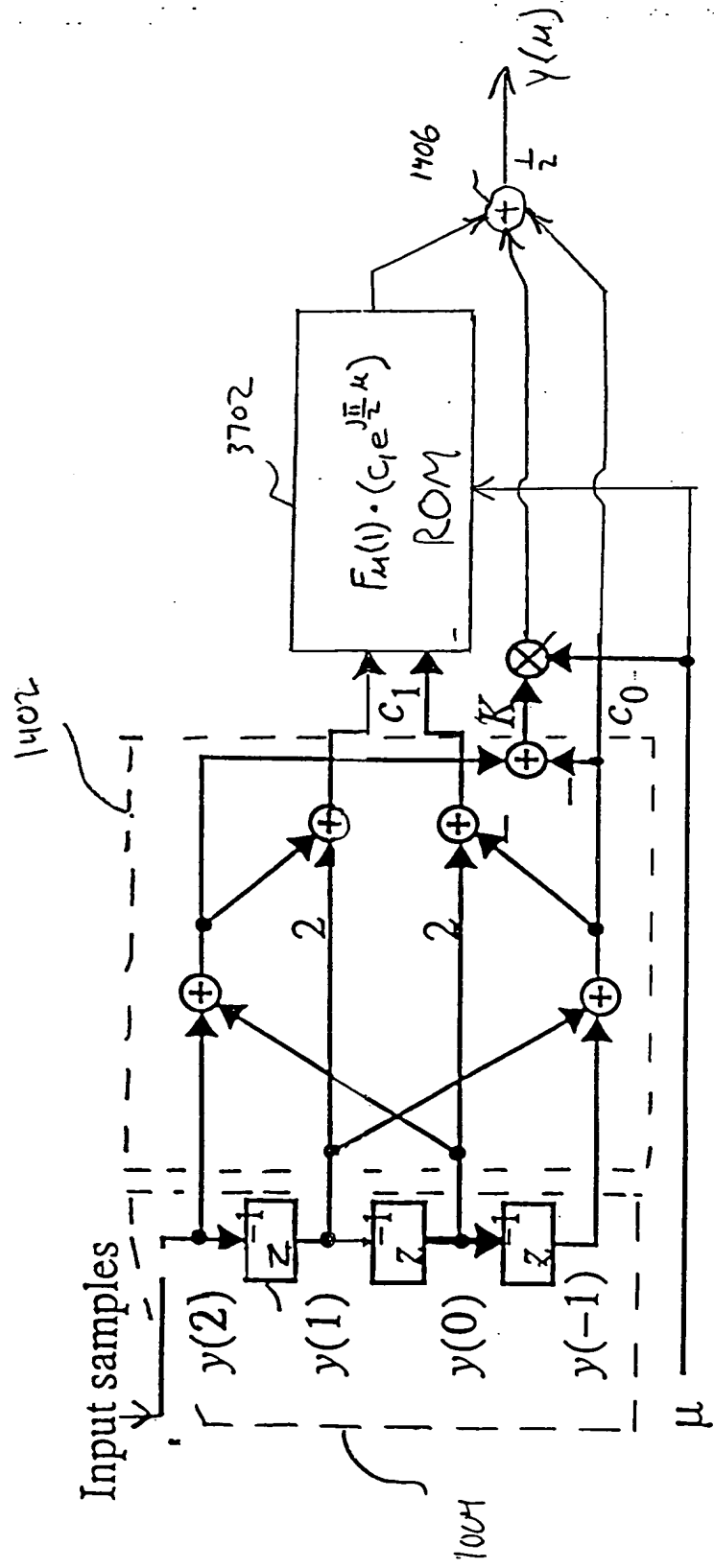


FIG.37 : The optimized structure for  $N=4$ .

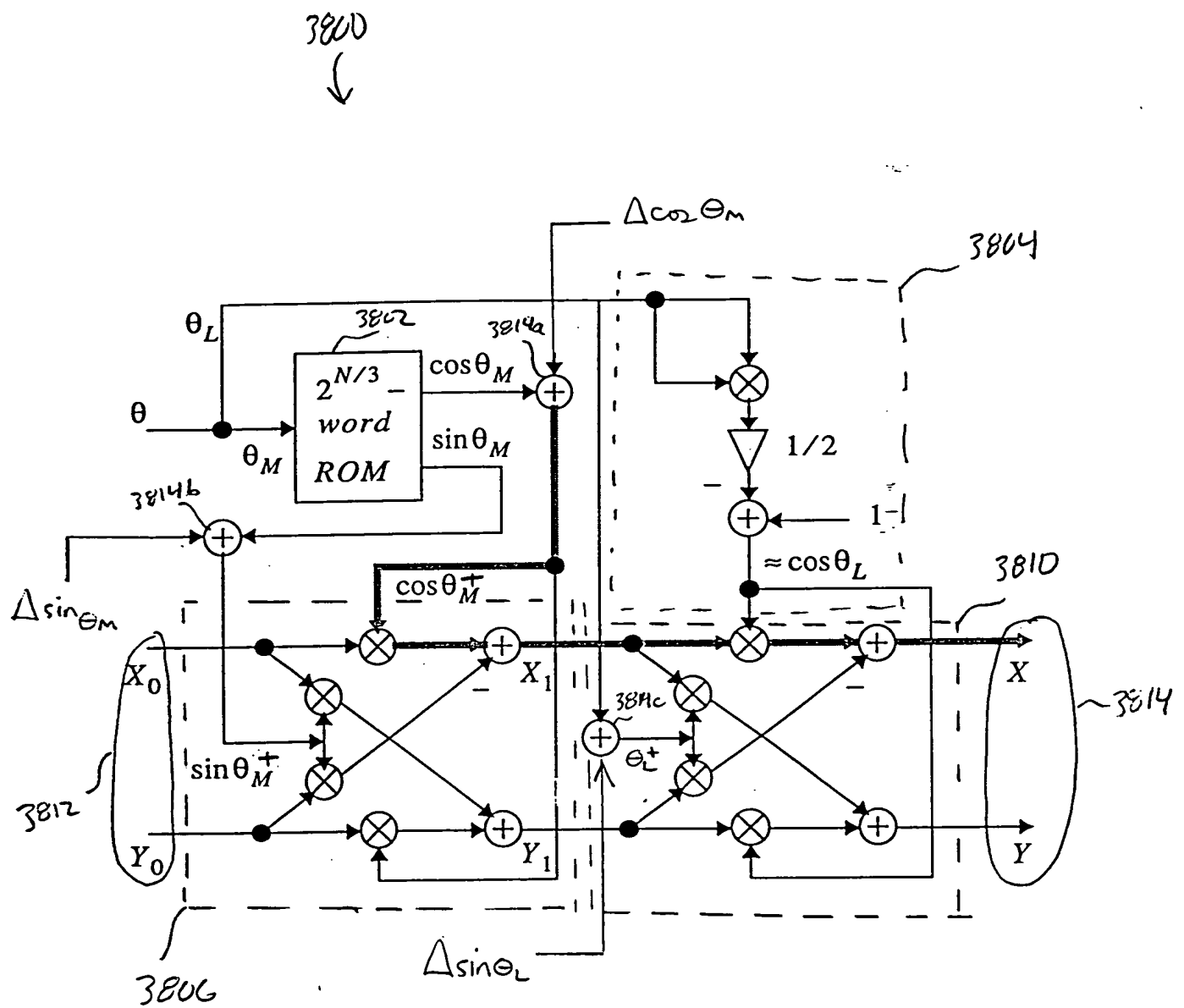


FIG. 38

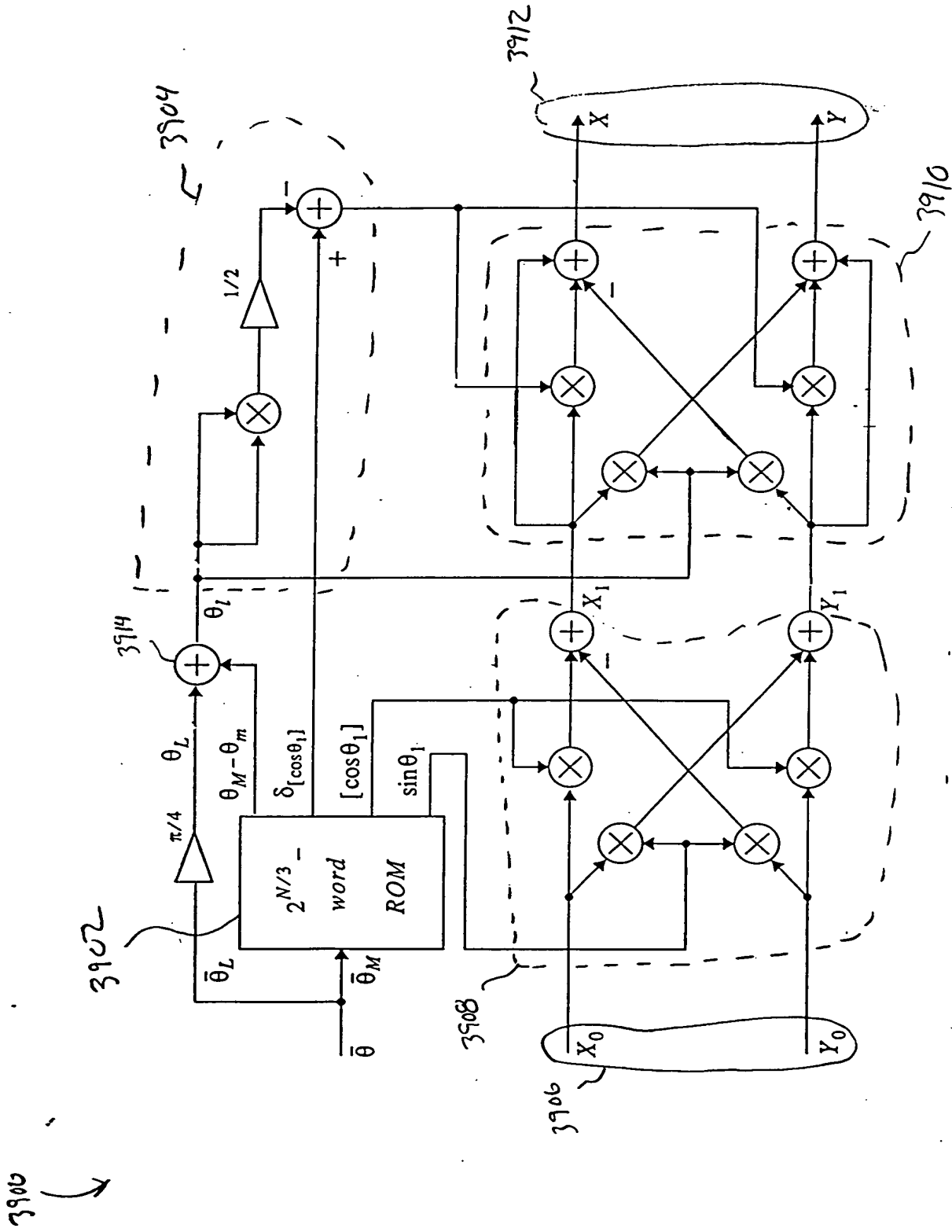


FIG. 39

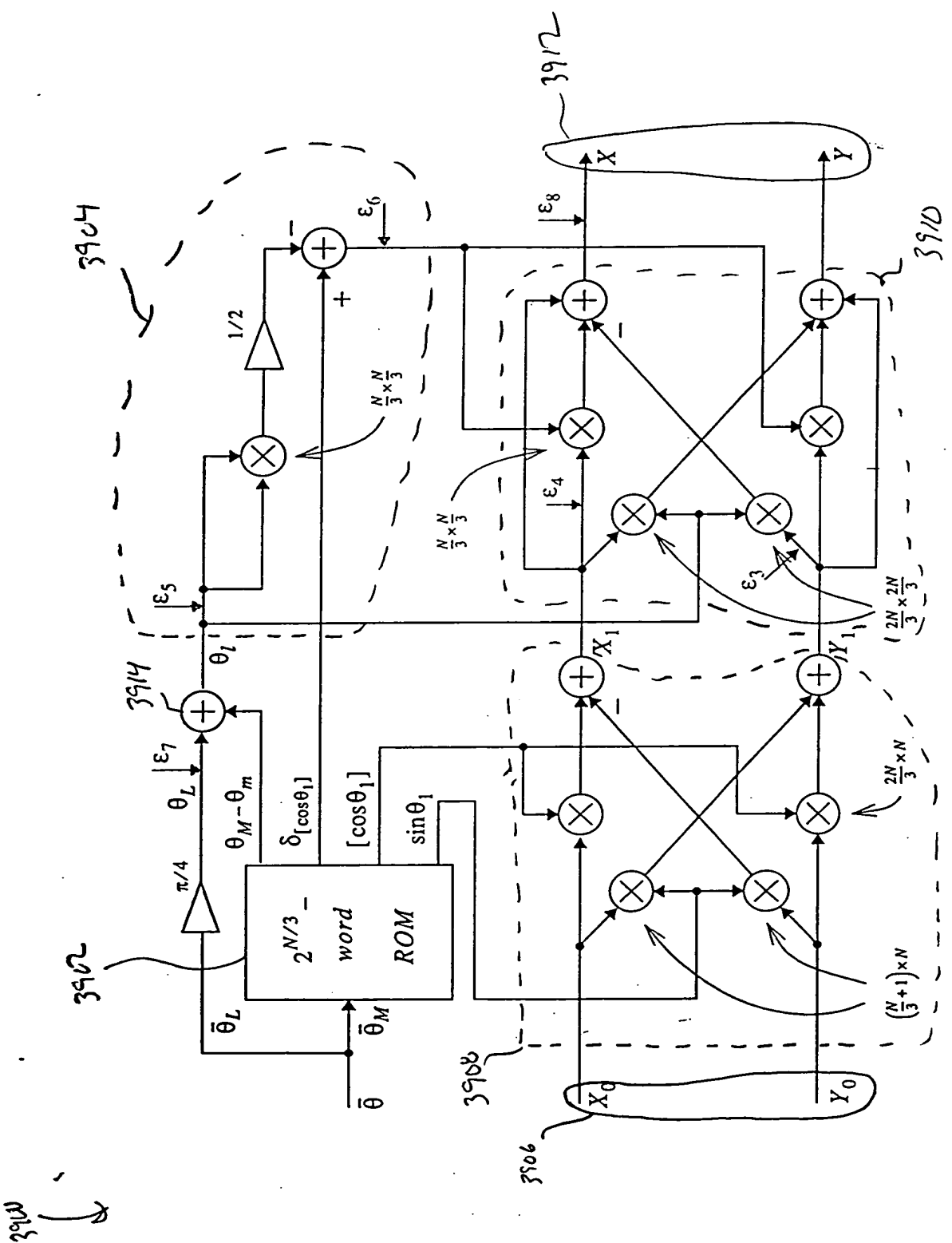


Fig. 40

00000010000000000000000000000000

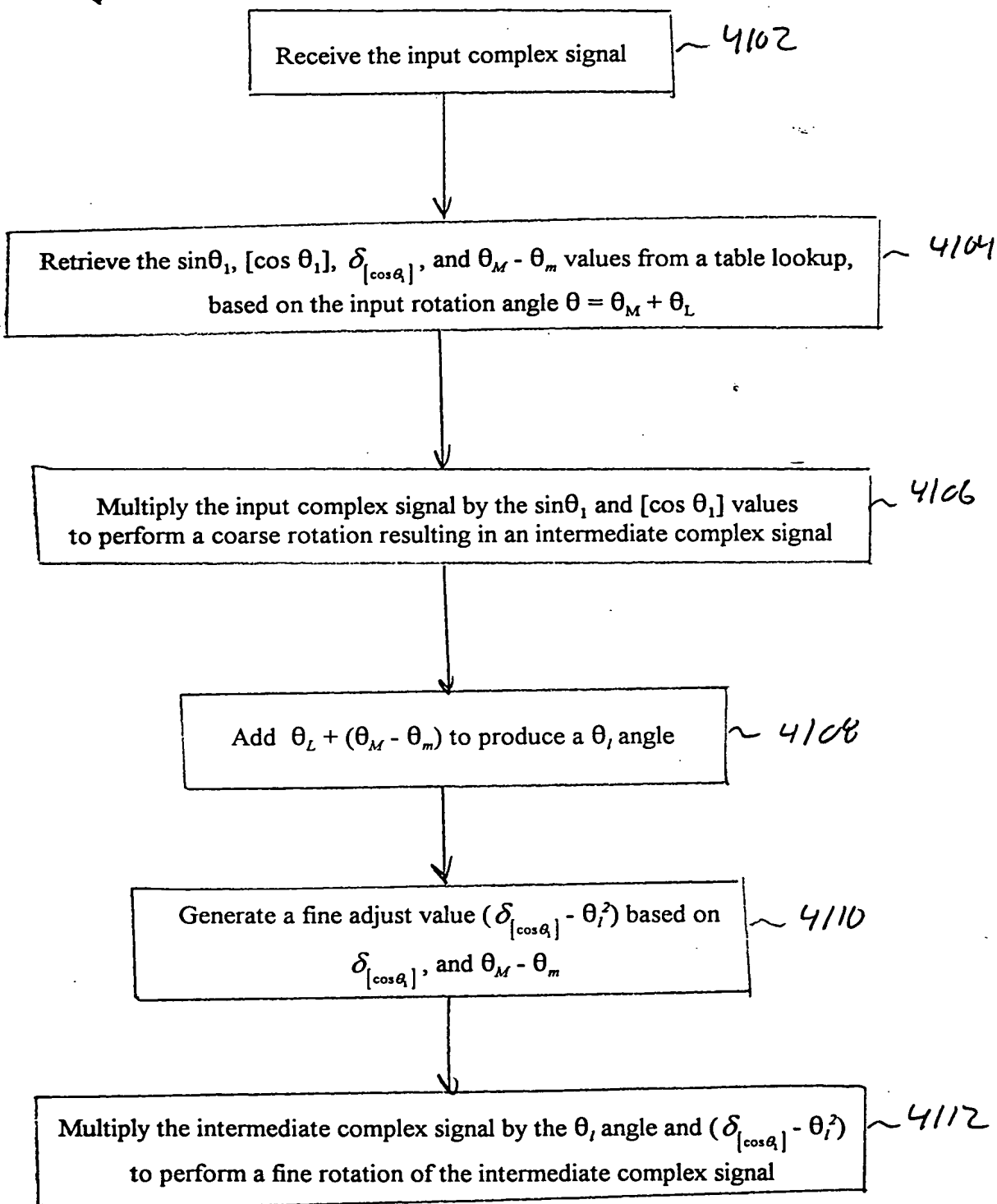
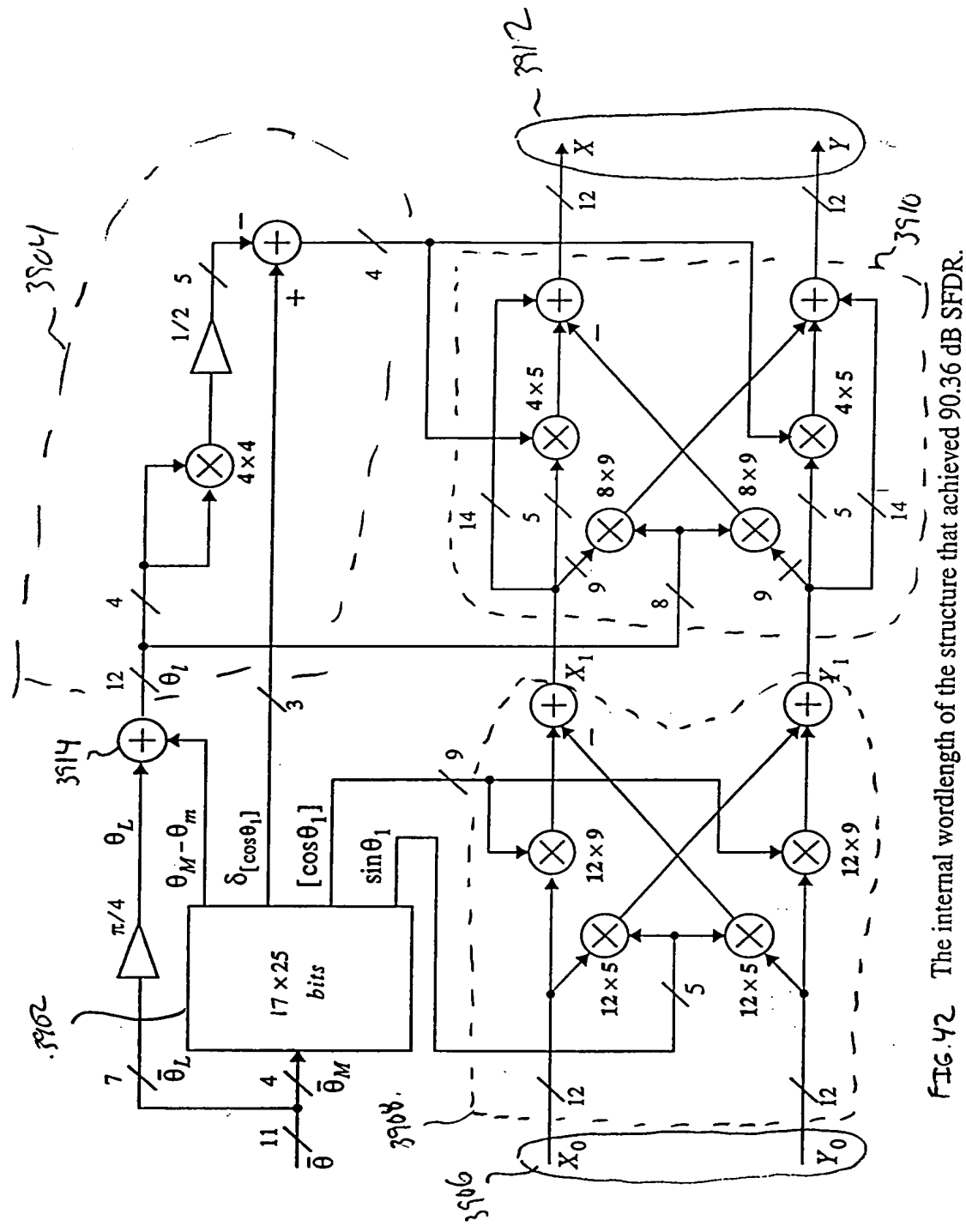


FIG. 41

卷之三

三九



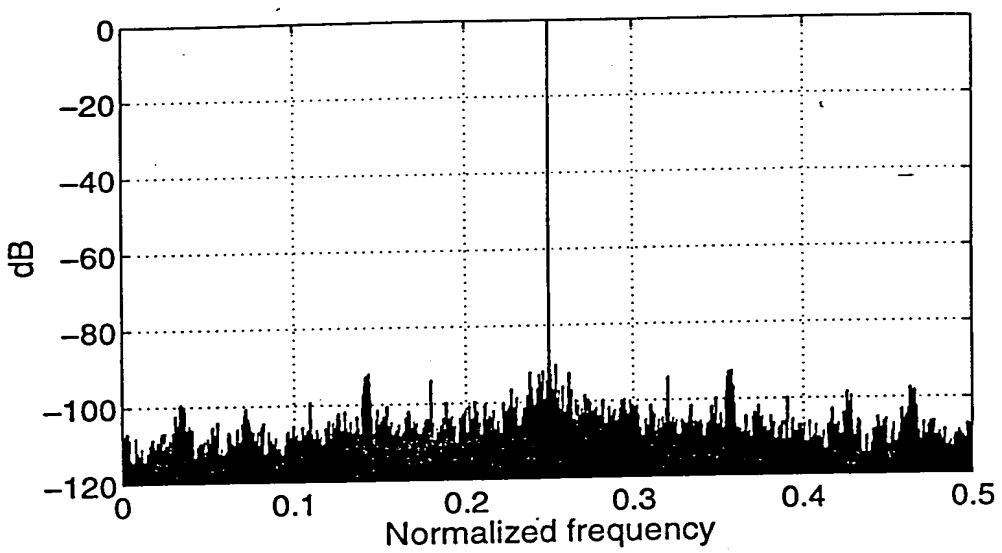
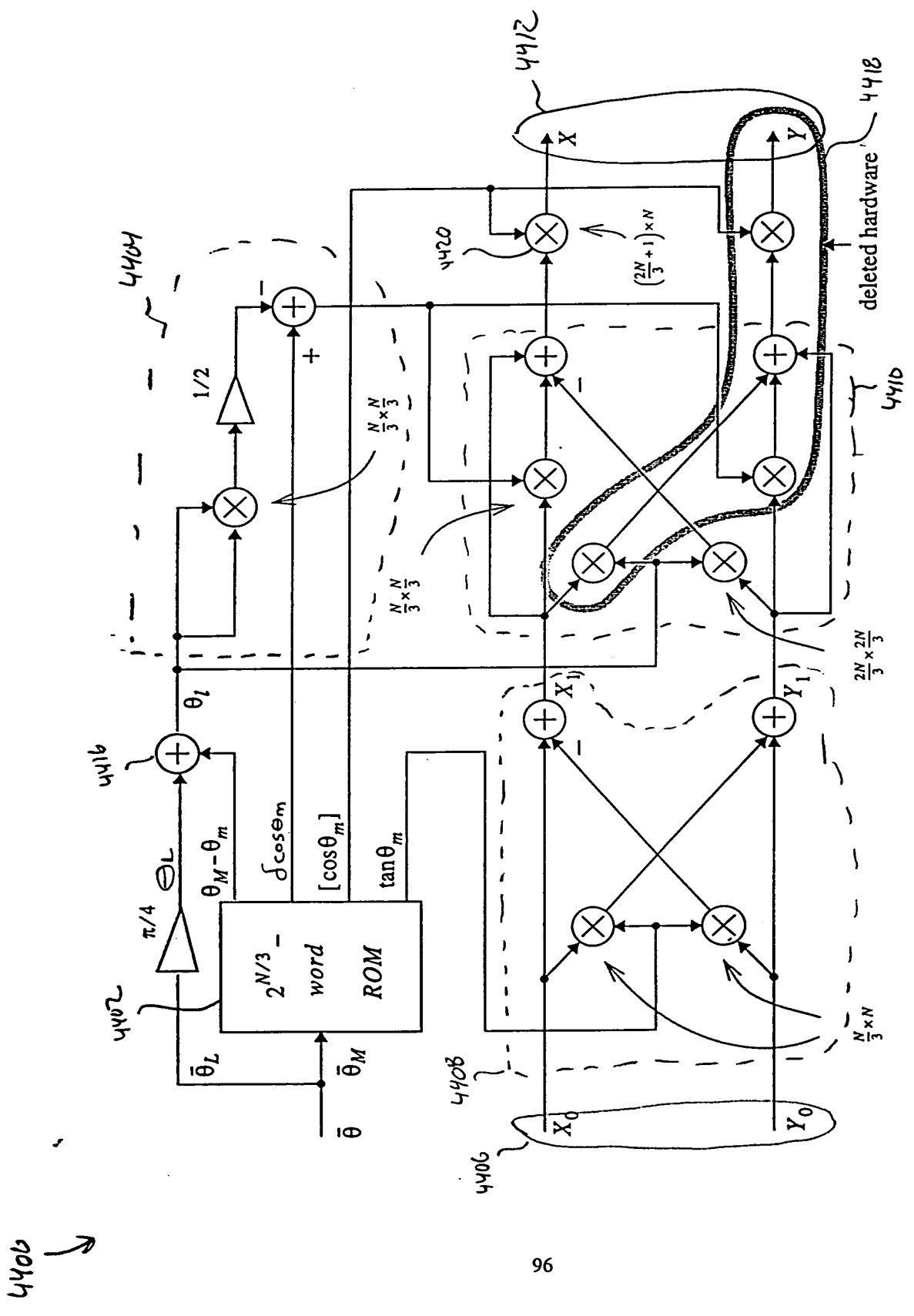


FIG. 43 Output spectrum showing 90.36 dB SFDR.



**FIG. 44** A modified architecture when only one output is needed.

4500

Receive the input complex signal

4502

Retrieve the  $\tan\theta_m$ ,  $[\cos\theta_m]$ ,  $\delta_{\cos\theta_m}$ , and  $(\theta_M - \theta_m)$  values from a table lookup, based on the input rotation angle  $\theta$

4504

Multiply the input complex signal by the  $\tan\theta_m$  value to perform a coarse rotation resulting in an intermediate complex signal

4506

Add  $\theta_L + (\theta_M - \theta_m)$  to produce a  $\theta_i$  angle

4508

Generate a fine adjust value ( $\delta_{\cos\theta_m} - \theta_i^2$ ) based on  $\delta_{\cos\theta_m}$ , and  $\theta_M - \theta_m$

4510

Multiply the intermediate complex signal by the  $\theta_i$  angle and  $(\delta_{\cos\theta_m} - \theta_i^2)$  to perform a fine rotation of the intermediate complex signal

4512

Scale the desired (X or Y) value of the output signal by  $[\cos\theta_m]$

4514

FIG. 45

460U

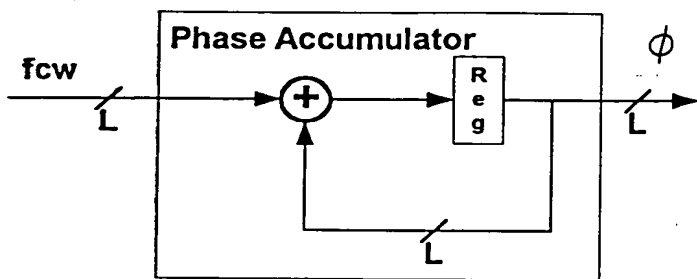


FIG. 46

where the adder is an overflowing  
accumulator.

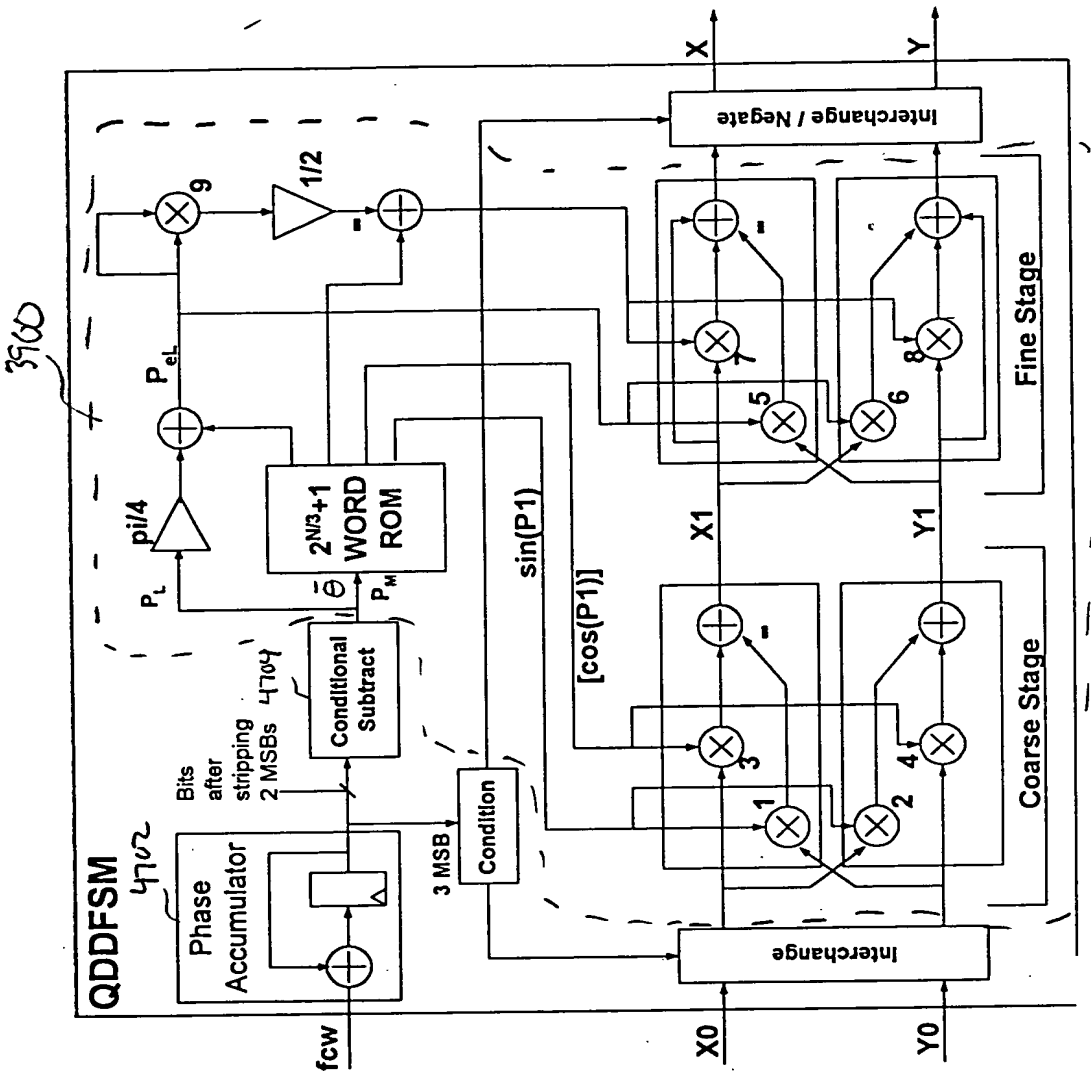
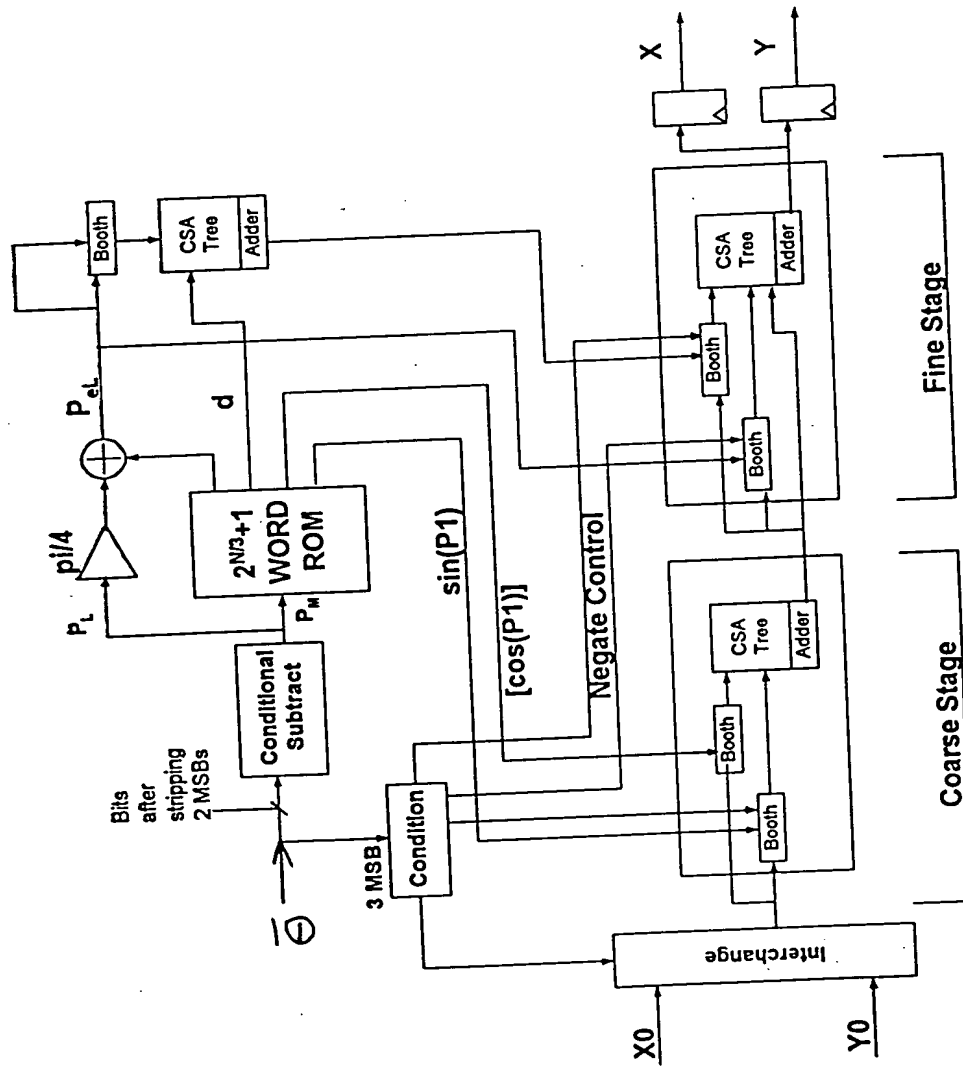


Fig. 48



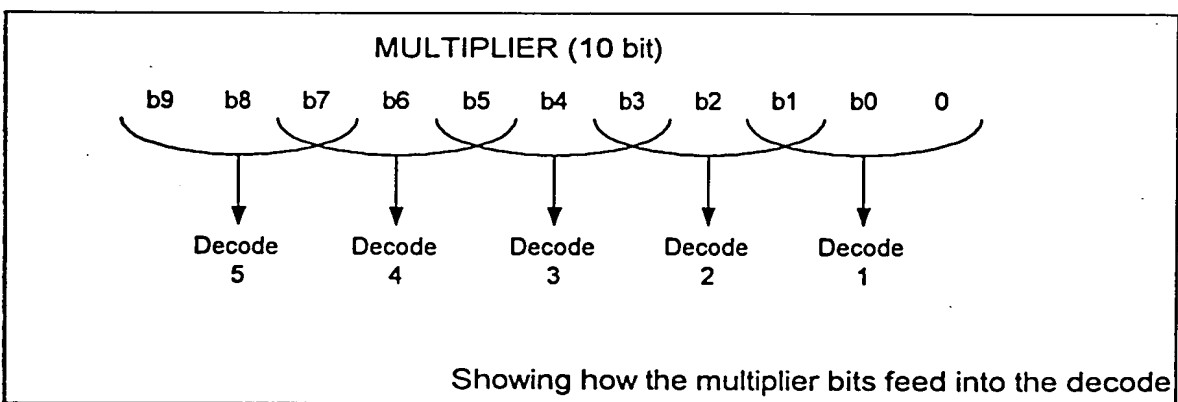
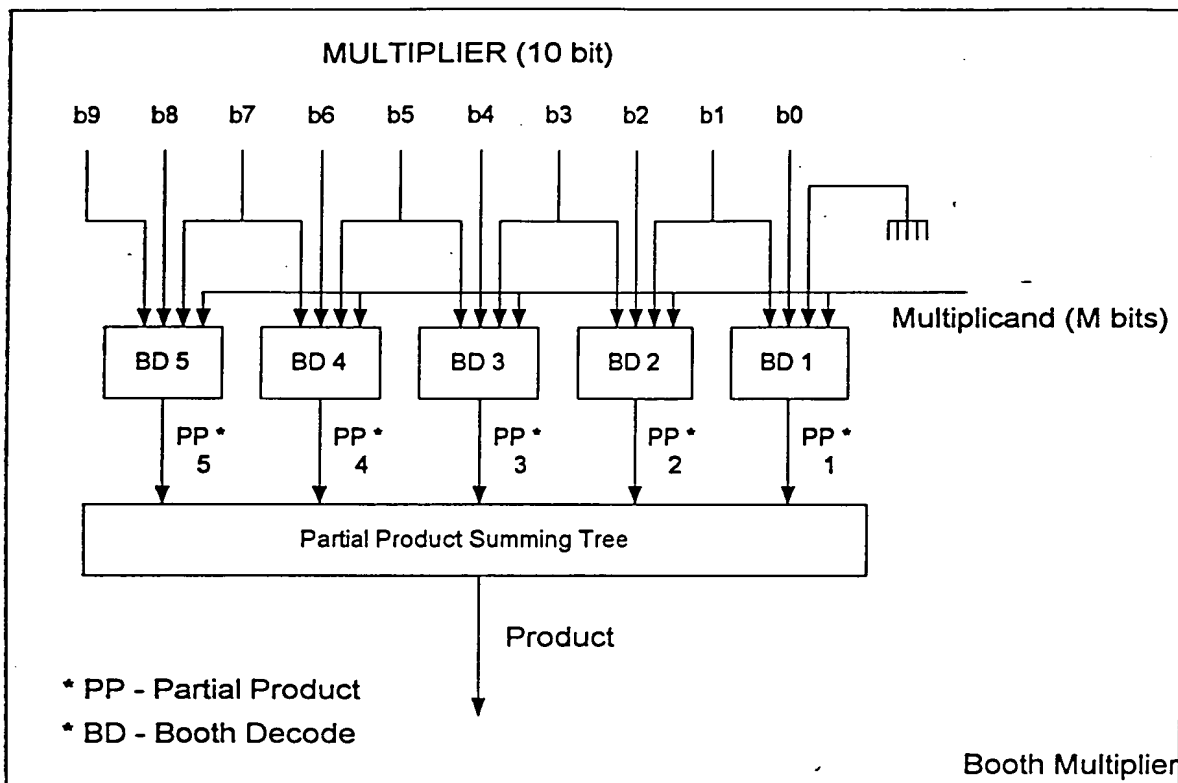


FIG. 49

5000  
↓

Original Booth Table

← 5002

b2 b1 b0 PP

0	0	0	$0^*A$
0	0	1	$1^*A$
0	1	0	$1^*A$
0	1	1	$2^*A$

5100  
↓

Negating Booth Table

← 5102

b2 b1 b0 PP

0	0	0	$0^*A$
0	0	1	$-1^*A$
0	1	0	$-1^*A$
0	1	1	$-2^*A$

1	0	0	$-2^*A$
1	0	1	$-1^*A$
1	1	0	$-1^*A$
1	1	1	$0^*A$

1	0	0	$2^*A$
1	0	1	$1^*A$
1	1	0	$1^*A$
1	1	1	$0^*A$

FIG. 50

FIG. 51

5266  
↓

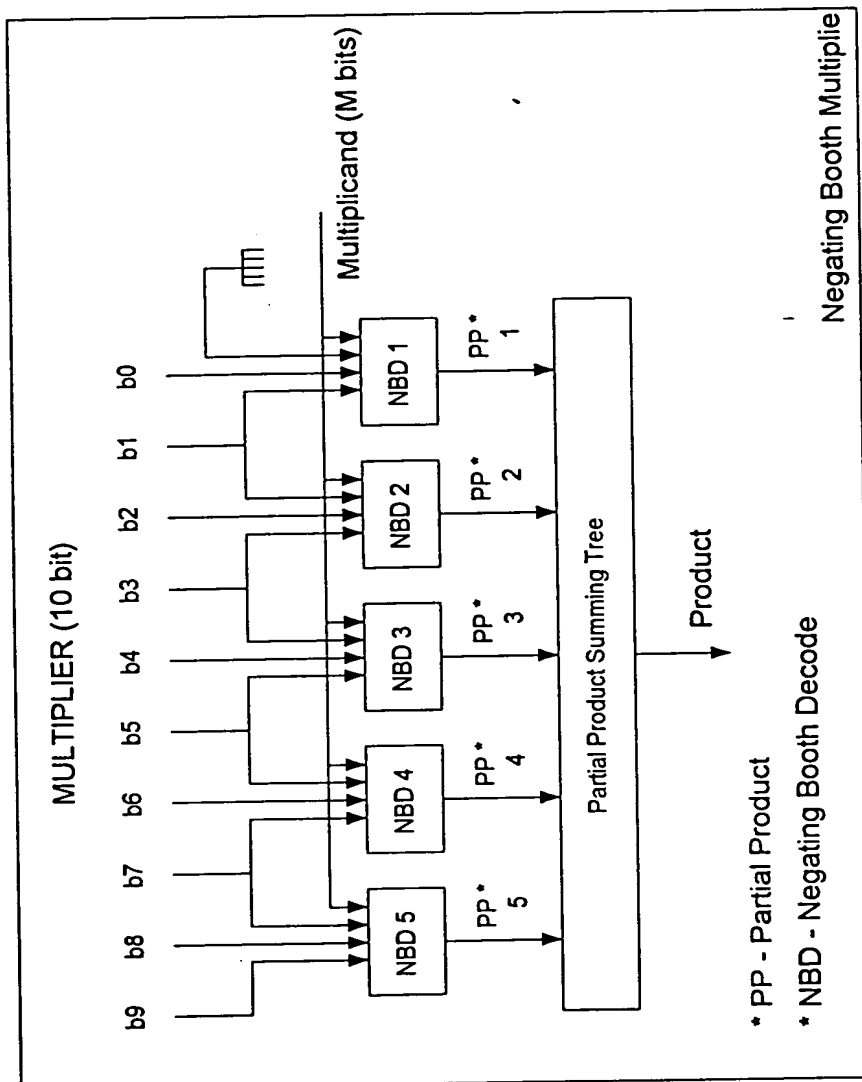


FIG. 52

5300

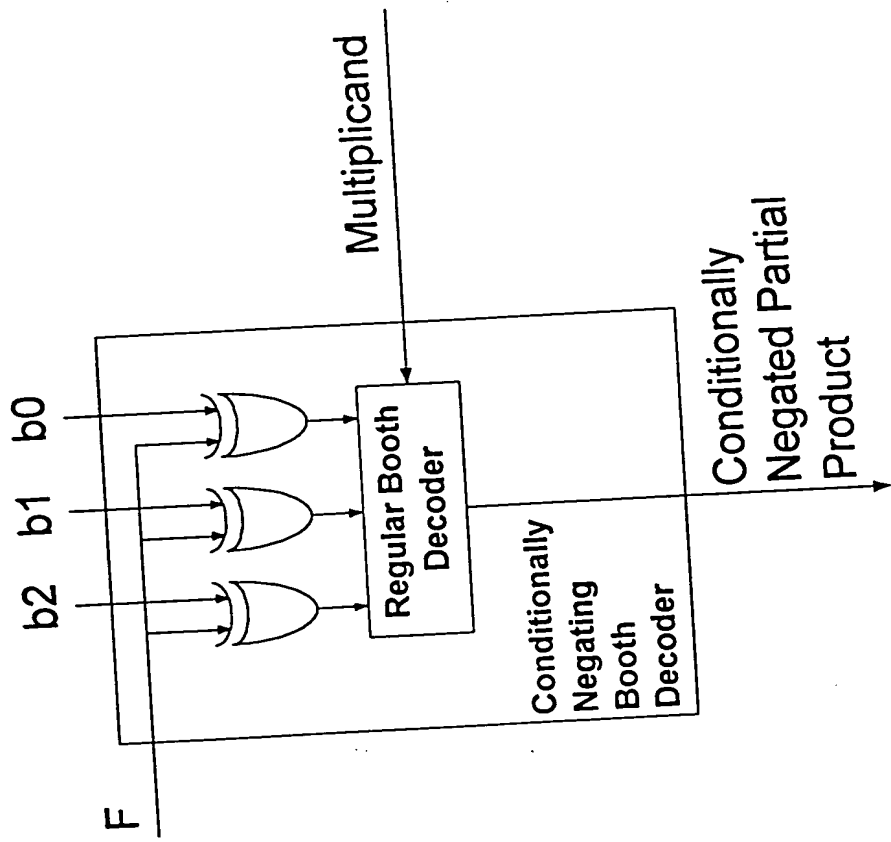


FIG. 53

54

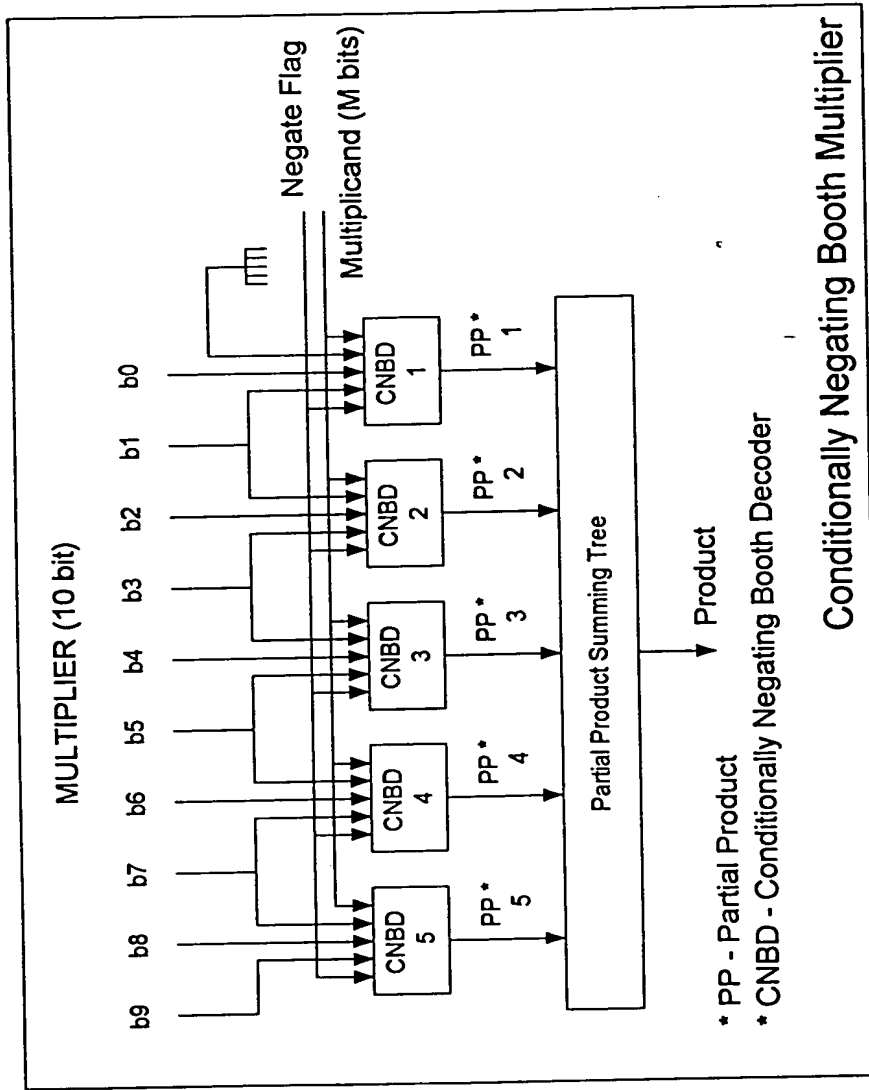


Fig. 54

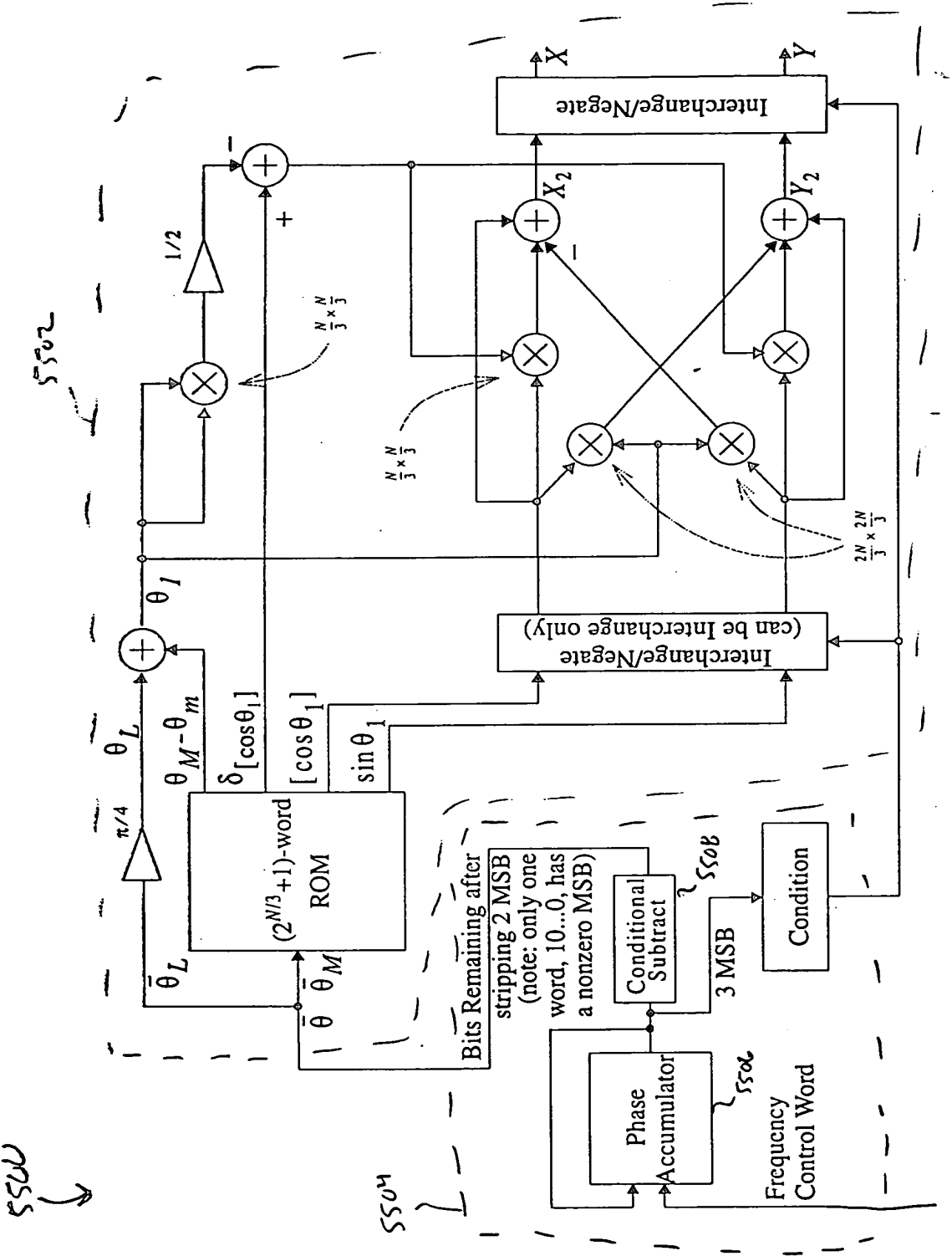
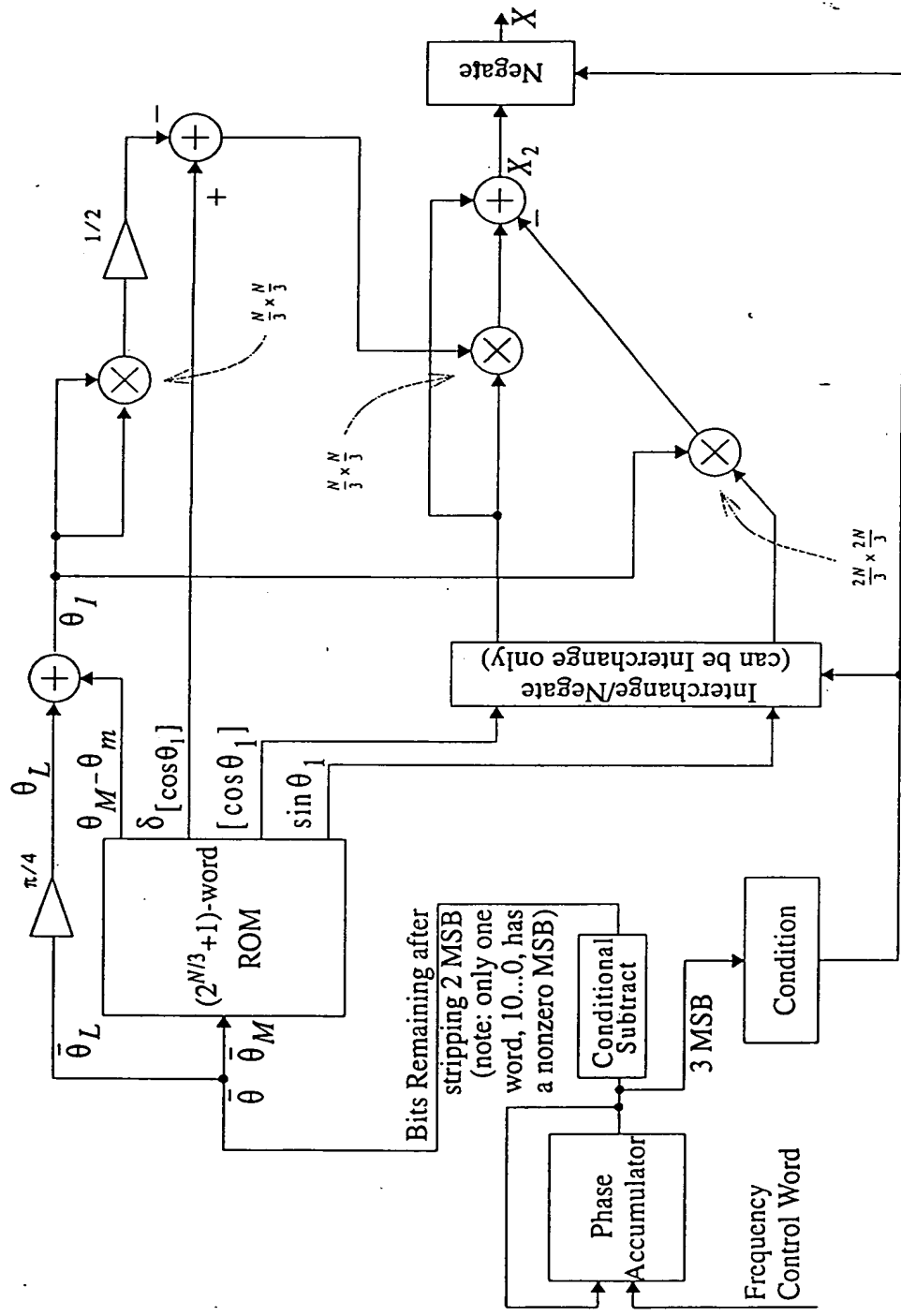


Fig. 55 Angle Rotator Configured as a Quadrature Direct Digital Synthesizer (QDDS).

二〇〇〇年九月二十一日

۵۶۰۶



**FIG. S6** Angle Rotator Configured as a “Cosine-only” Direct Digital Synthesizer (DDSS) {from Fig 39}.

$\zeta \tau \omega$

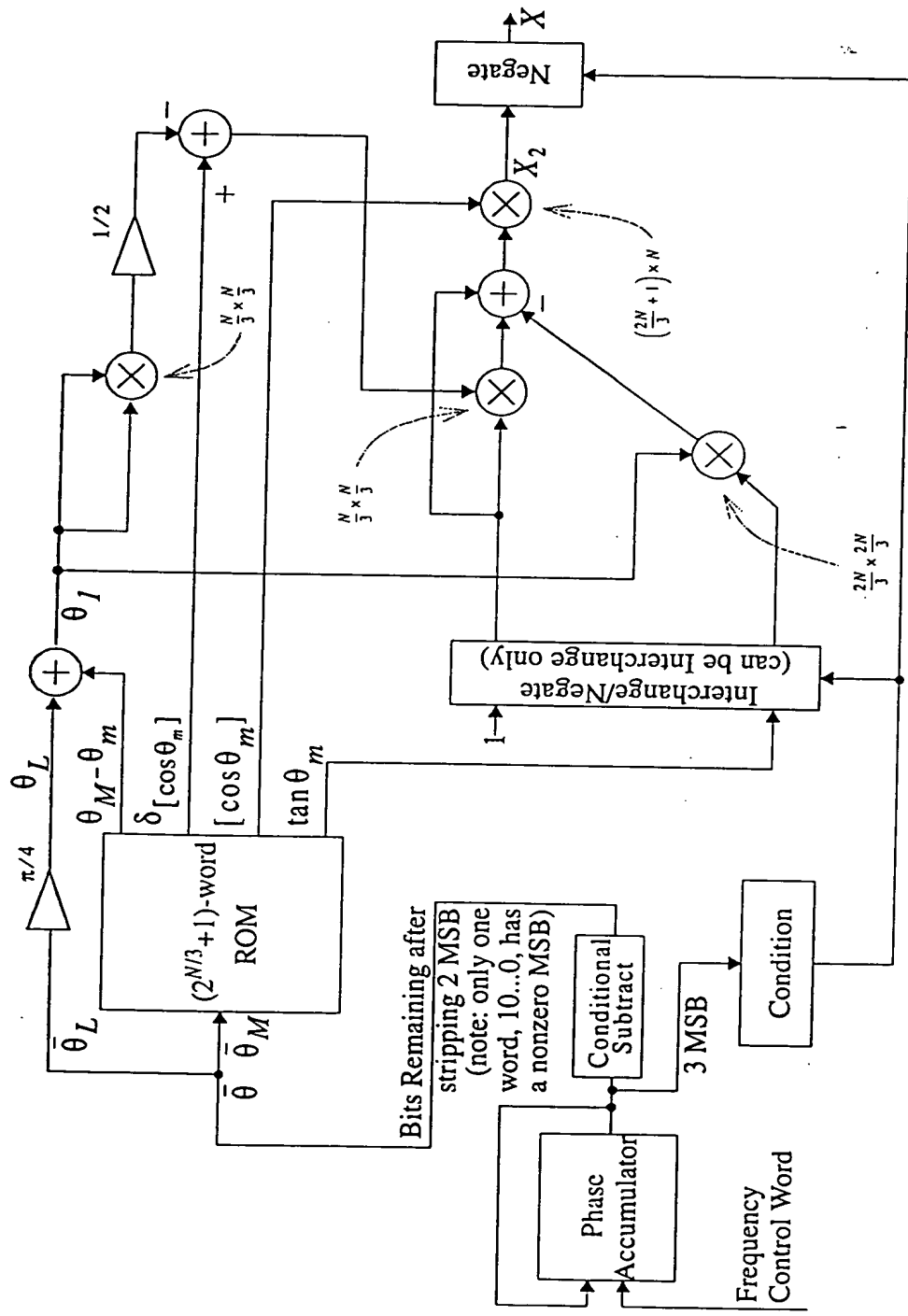


Fig. 57 Angle Rotator Configured as a "Cosine-only" Direct Digital Synthesizer (DDS) (from Fig. 44).

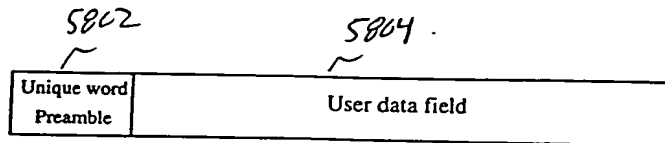


FIG. 58: Common packet format.

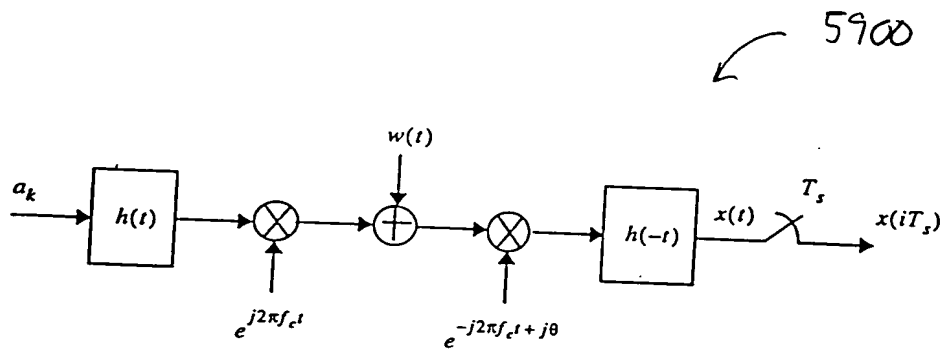


FIG. 59: The simplified system model.

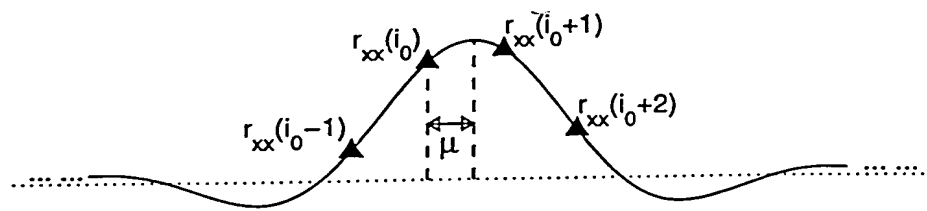


FIG. 60 Mean values of the preamble correlator output, for  $\theta = 0$ .

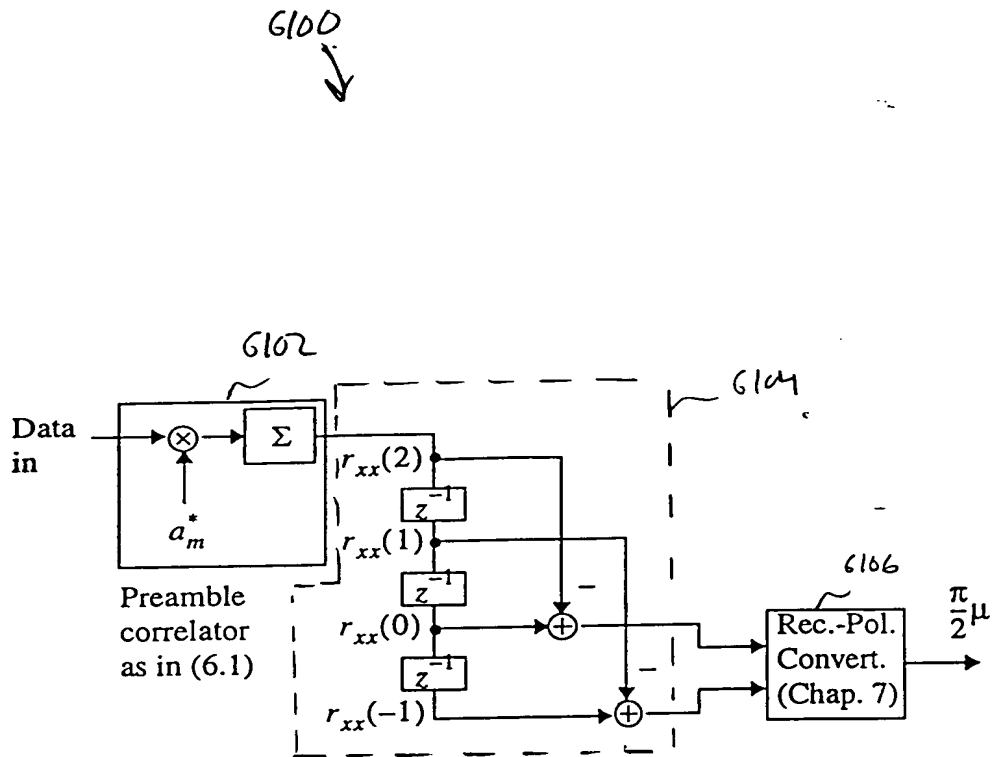


FIG. 61° Preliminary symbol-timing estimation structure.

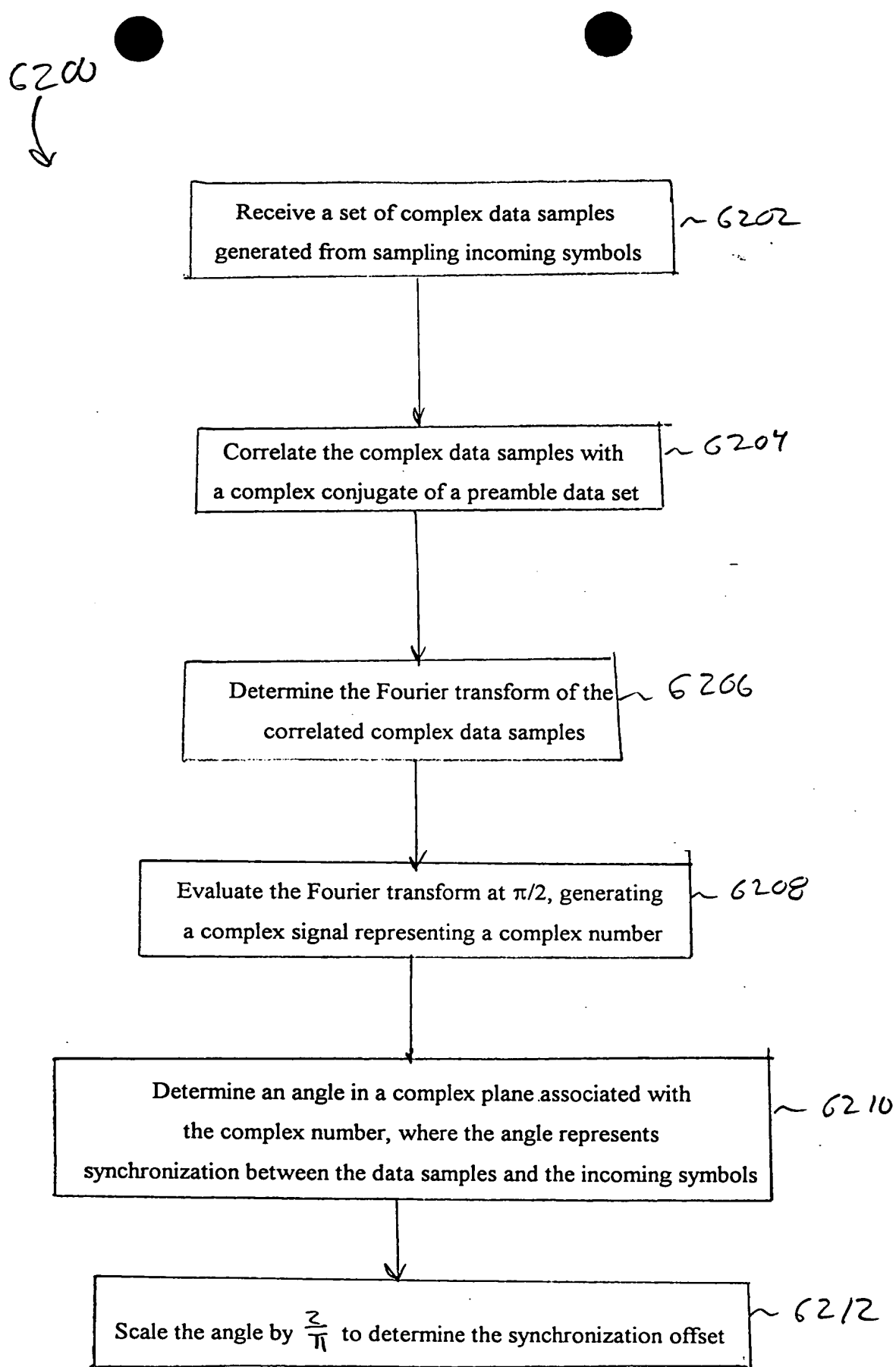


FIG. 62

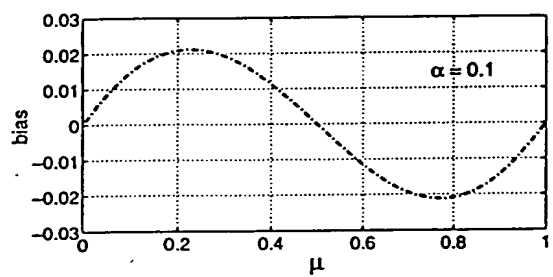


FIG. 63 Bias due to truncation.

6400

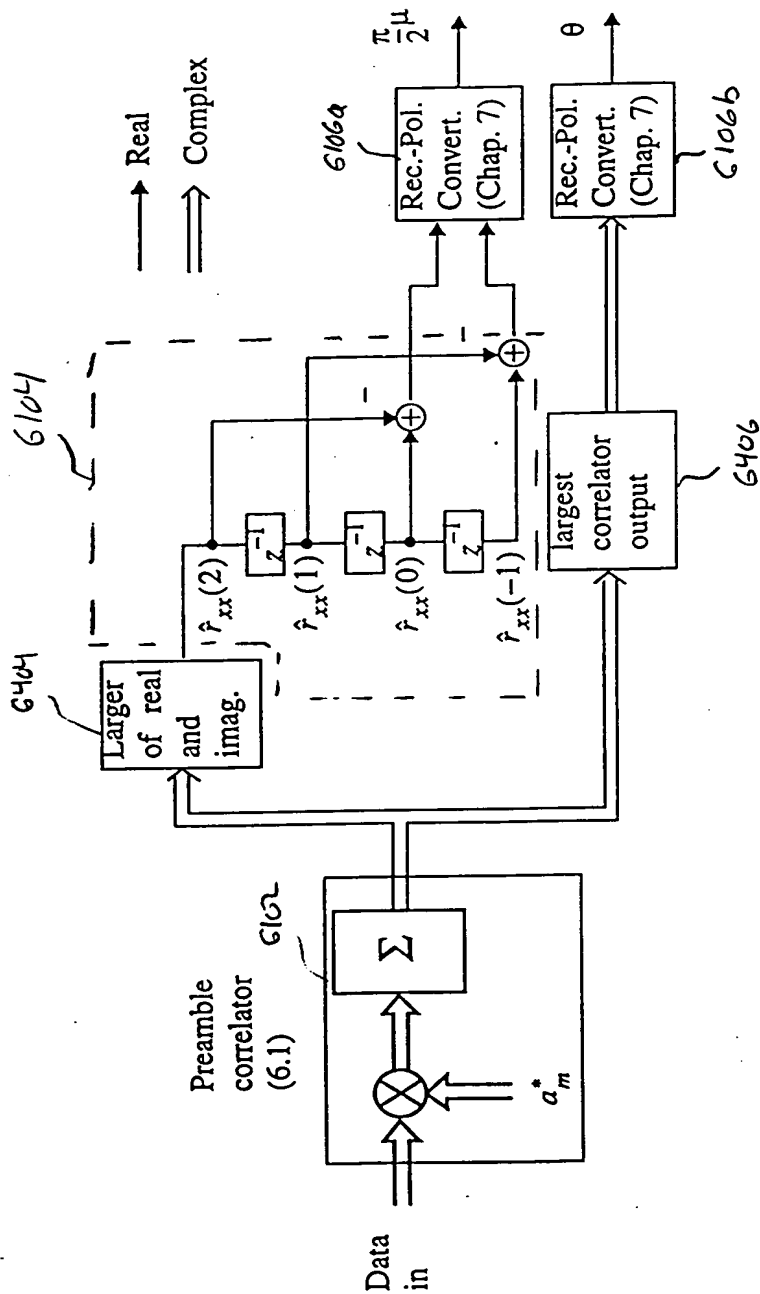


Fig. 64 Structure for carrier-phase and symbol timing recovery.

6500



Receive a set of complex data samples generated from sampling incoming symbols

6502

Correlate the data samples with a complex conjugate of a preamble data set

6504

Select either the set of real correlated samples or the set of imaginary correlated samples based on magnitude

6506

Determine the Fourier transform of the selected correlated samples

6508

Evaluate the Fourier transform at  $\pi/2$ , generating a complex signal representing a complex number

6510

Determine an angle in the complex plane associated with the complex number of step 6510, where the angle represents synchronization between the data samples and the incoming symbols

6512

FIG. G 5A

6504 (cont.)

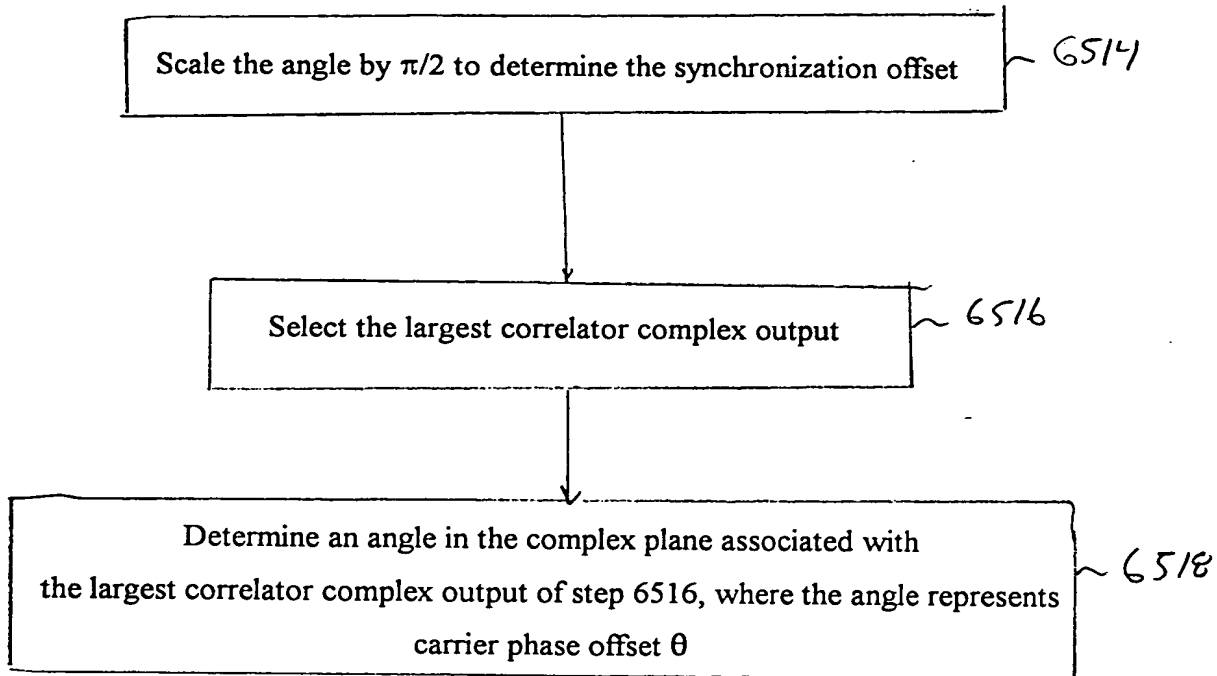


FIG. 65B

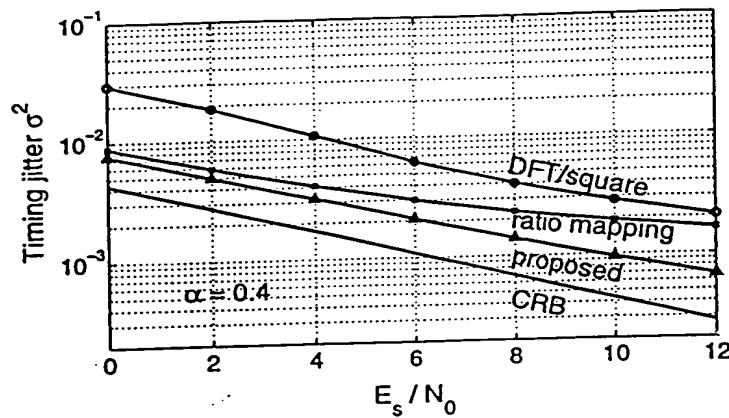


Figure 66: Timing jitter variance,  $\alpha = 0.4$ .

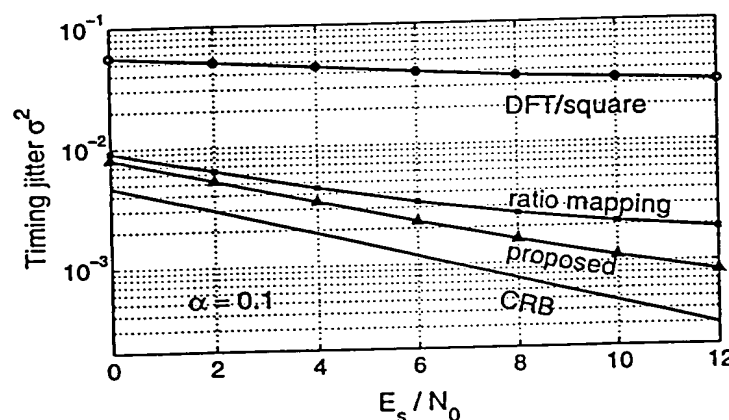


Figure 67: Timing jitter variance,  $\alpha = 0.1$ .

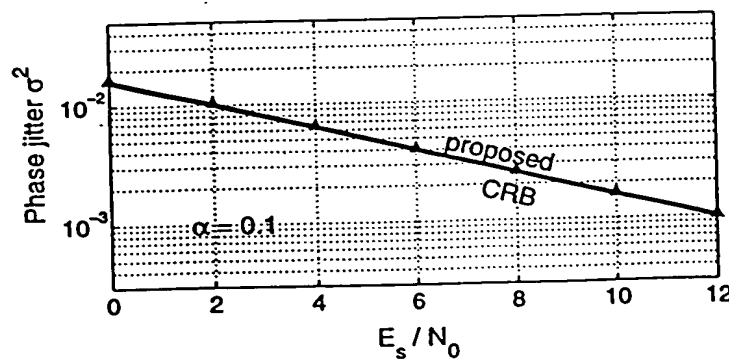


Figure 68: Phase jitter variance,  $\alpha = 0.1$ .

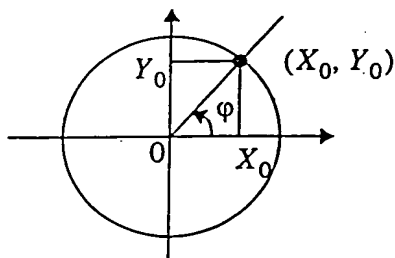


FIG. G1    Cartesian to polar conversion.

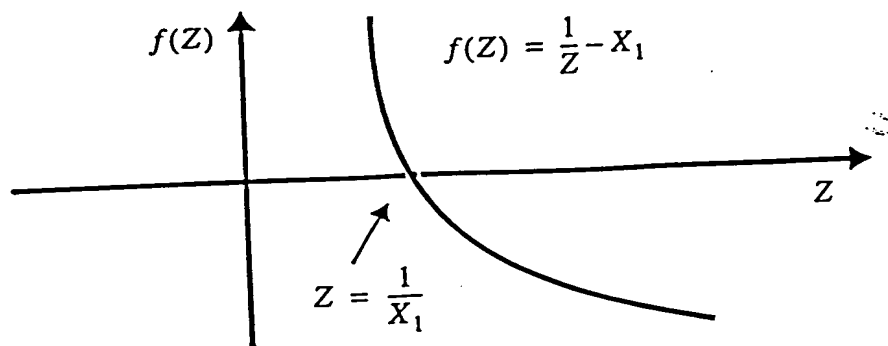


FIG. 70A: Using Newton-Raphson iteration to find  $1/X_1$ .

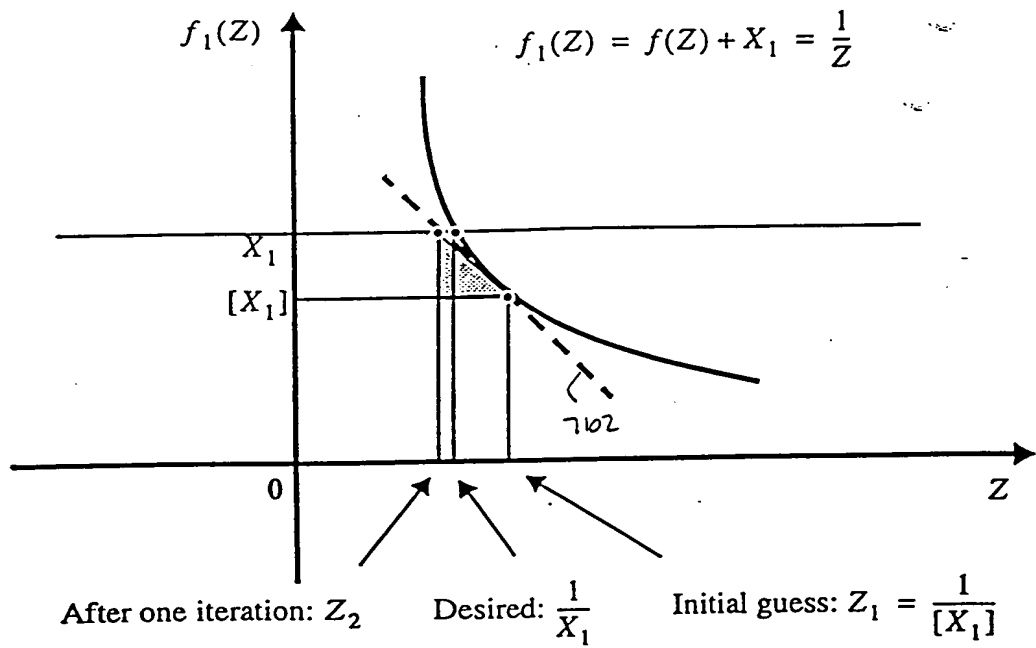


FIG. 70B: One Newton-Raphson iteration.

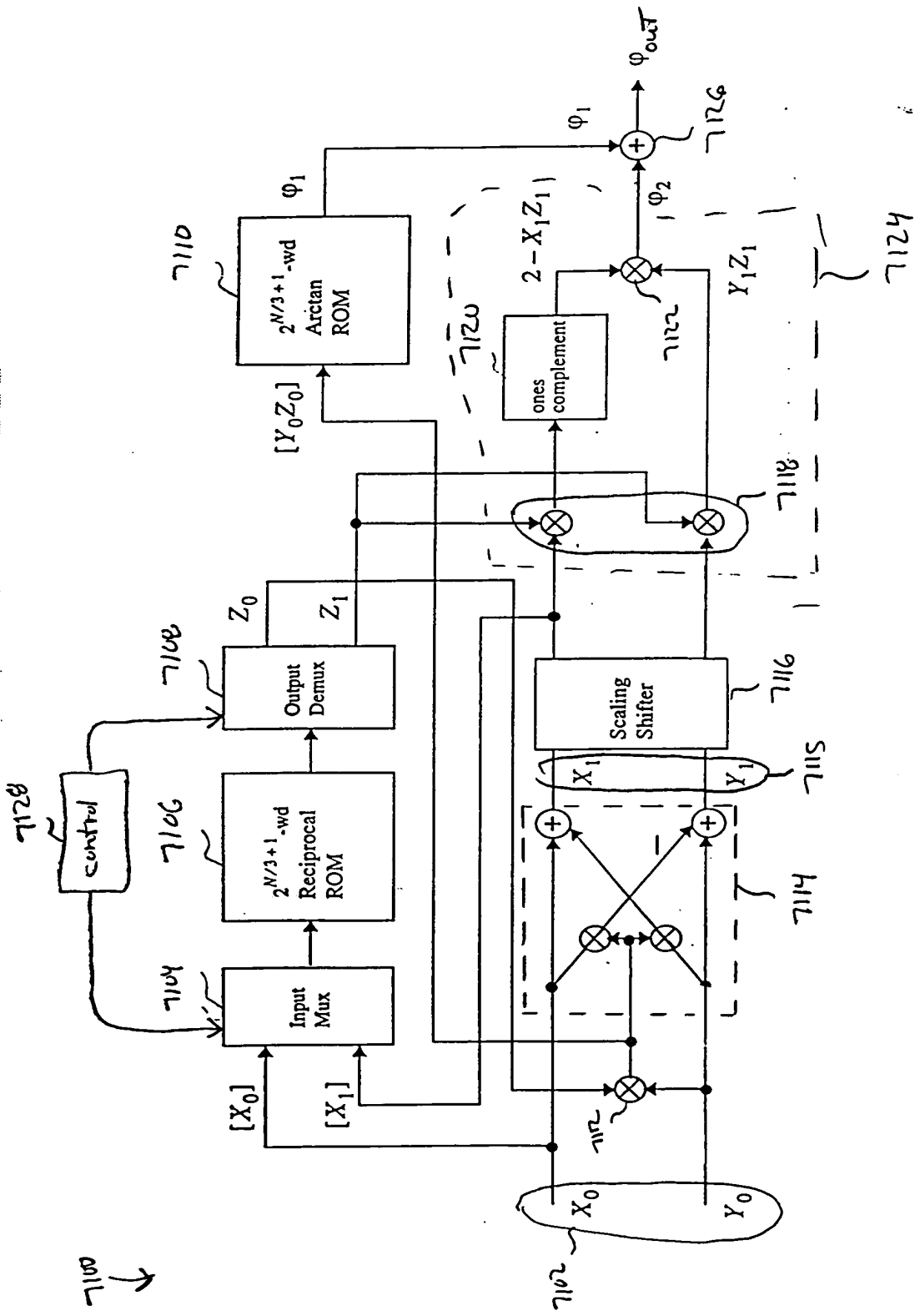


FIG. 71:

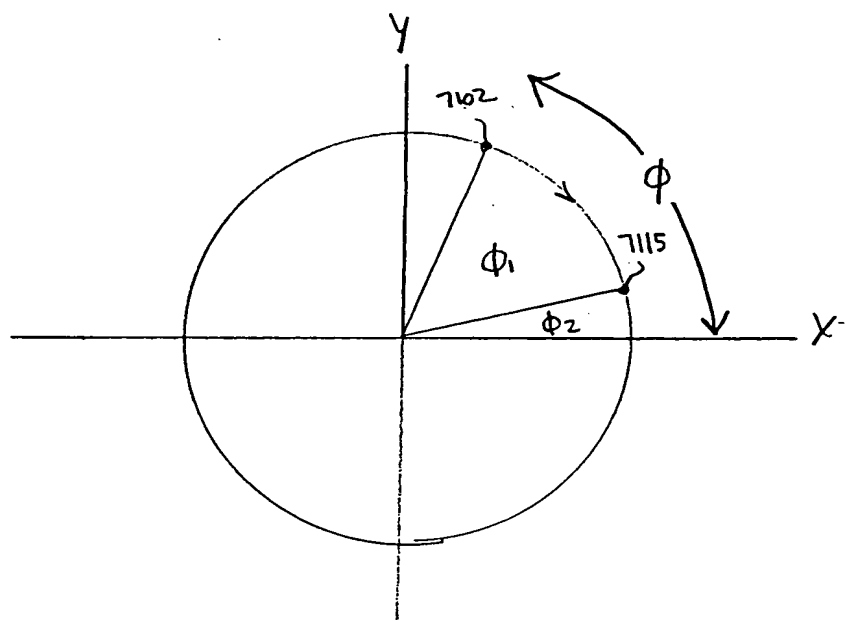
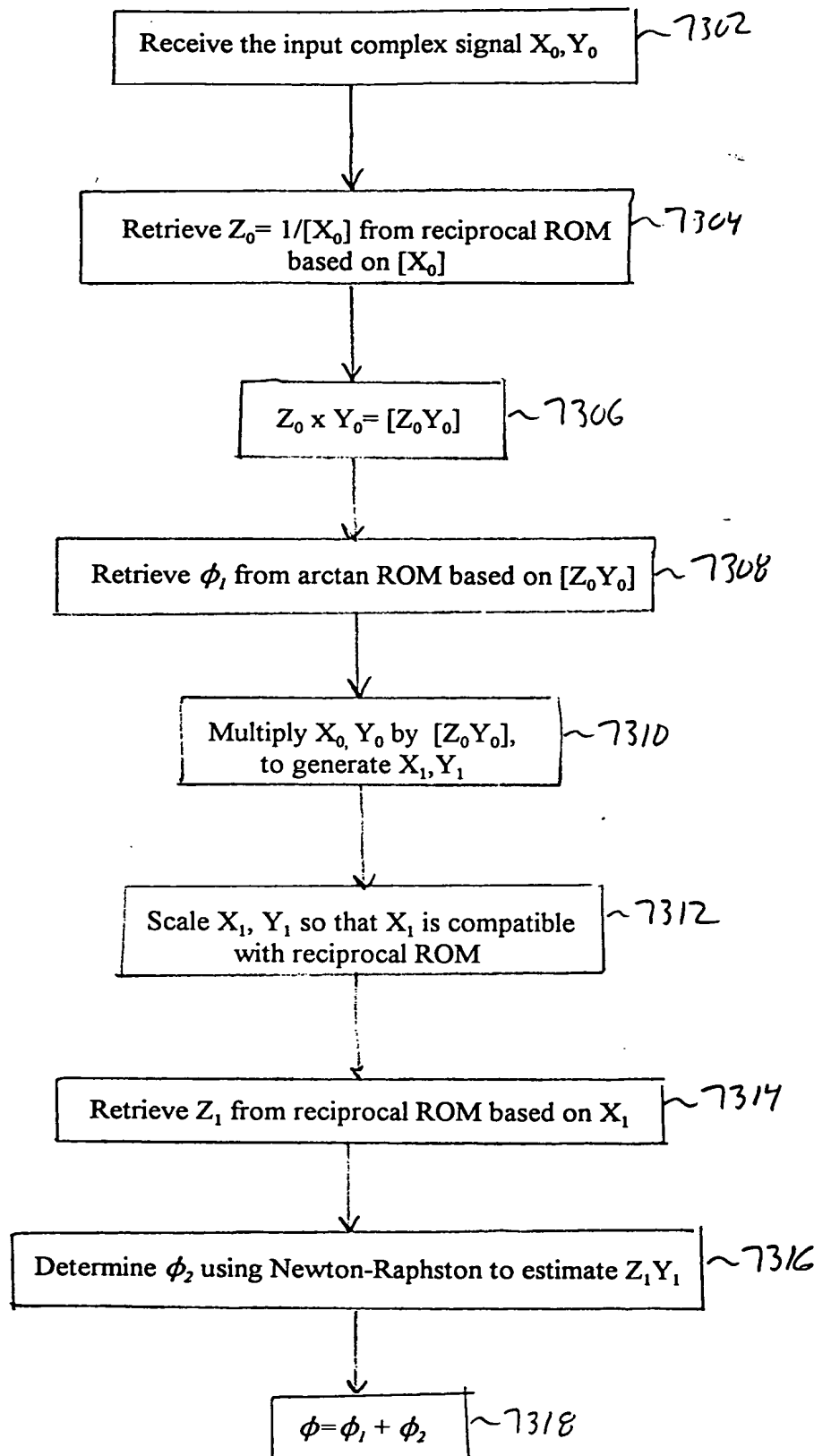


FIG. 72

7300

FIG. 73

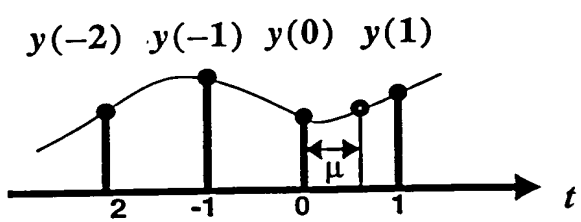


FIG. 74 Interpolation in a non-center interval.

FIG.75A

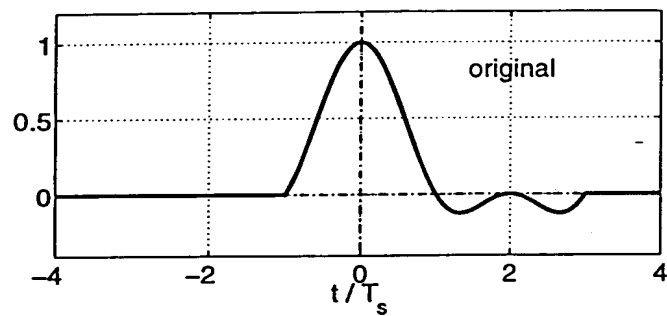


FIG 75B

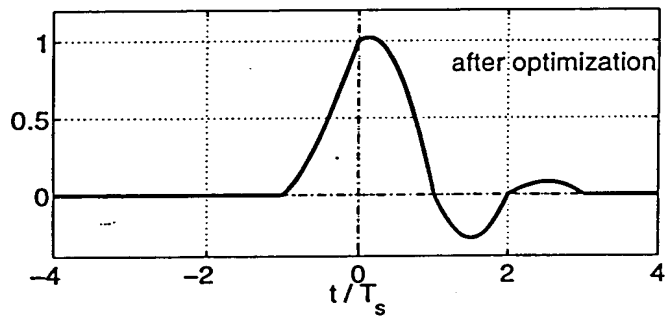


FIG.75A-B: Impulse responses of the non-center-interval interpolation filter  $\mathcal{A}$  before and  $\mathcal{B}$  after optimization.

FIG. 76A

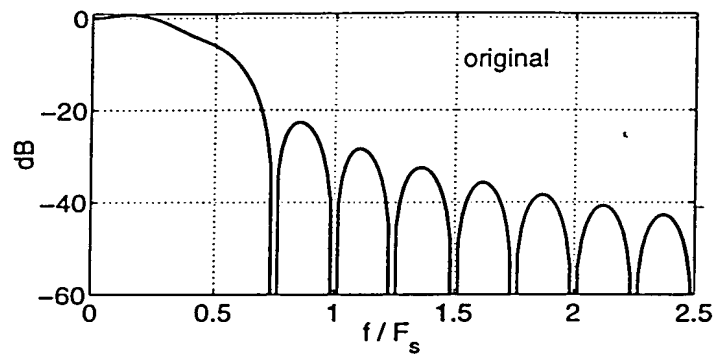


FIG. 76B

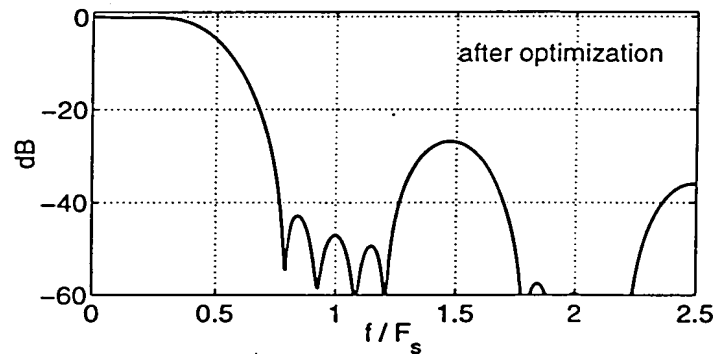


FIG. 76A - B : Frequency responses of the non-center-interval interpolator before optimization , after optimization.

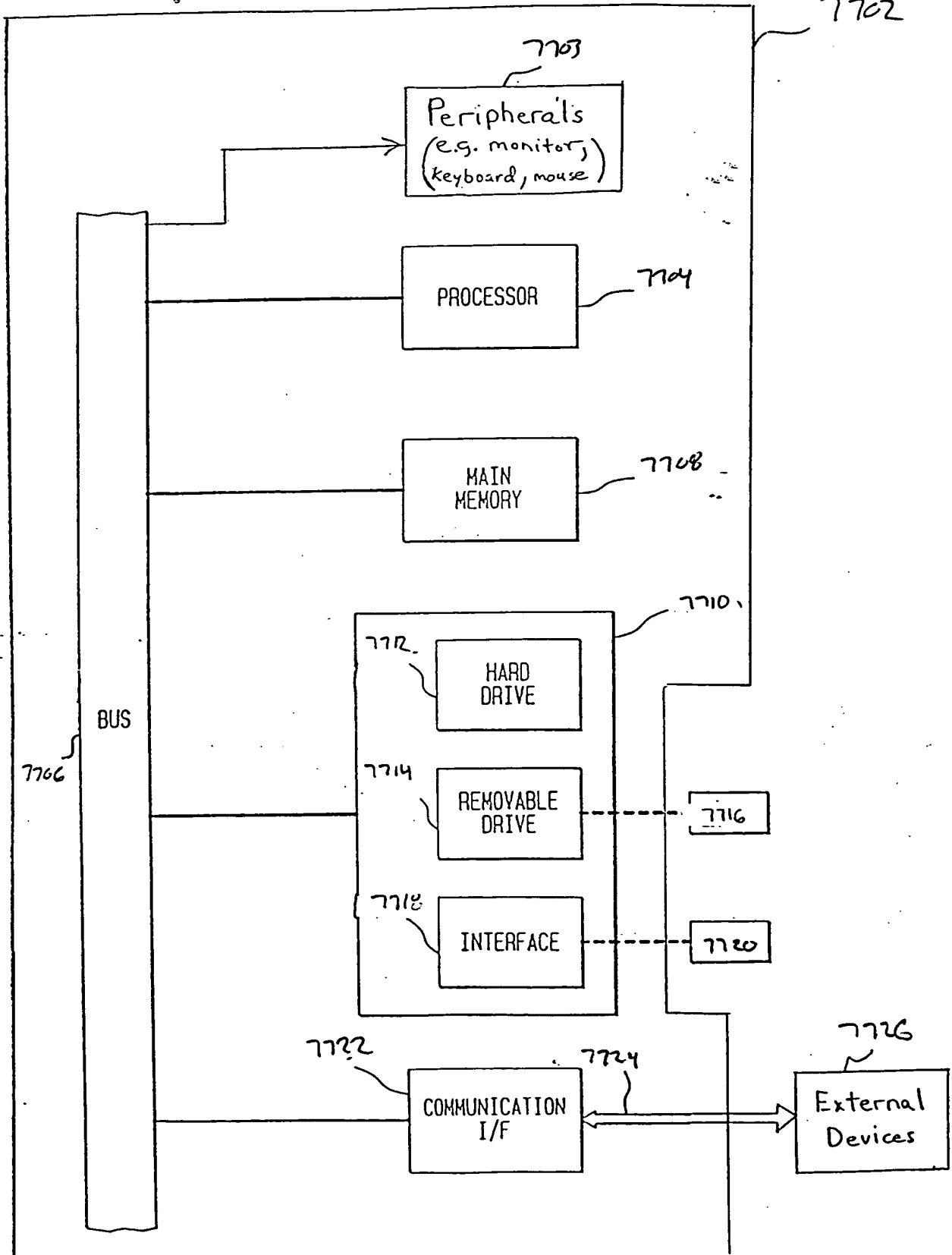


FIG. 77

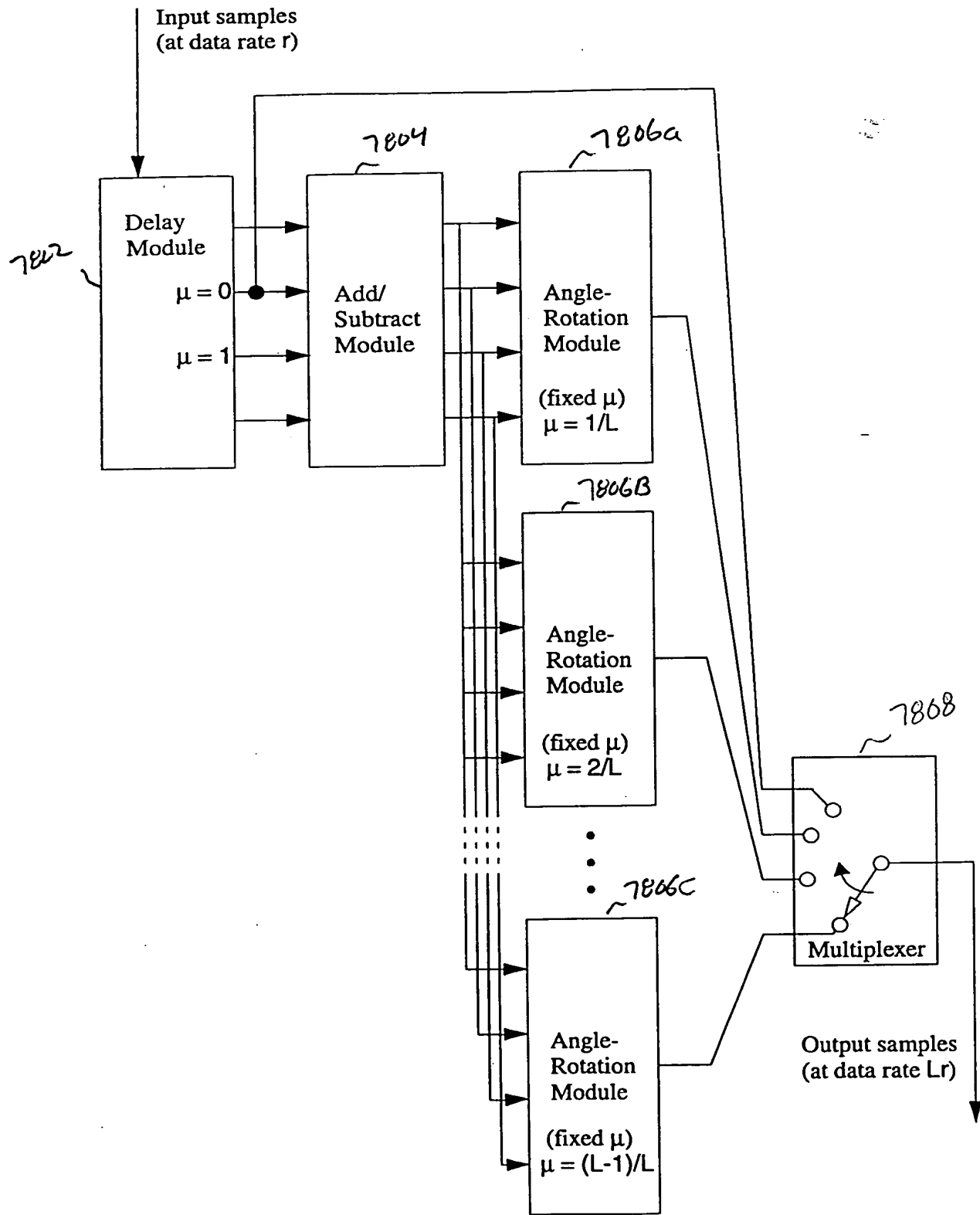


FIG. 78 Data Rate Expansion Circuit.